Geol. Mag. **142** (*1*), *2005, pp. 109–130. © 2005 Cambridge University Press*
DOI: 10.1017/S0016756804009951 *Printed in the United Kingdom*

Petrology and geochronology of Mesoproterozoic mafic–intermediate plutonic rocks from Mitwaba (D. R. Congo): implications for the evolution of the Kibaran belt in central Africa

J. KOKONYANGI*†, A. B. KAMPUNZU‡, M. POUJOL¶, T. OKUDAIRA*, M. YOSHIDA§ & K. P. SHABEER*

*Department of Geosciences, Osaka City University, Osaka 558-8585, Japan
‡University of Botswana, Department of Geology, Private Bag 0022, Gaborone, Botswana
¶Department of Earth Sciences, Memorial University of Newfoundland, St John's, NF A1B 3X5, Canada
§Gondwana Institute for Geology and Environment, 147-2 Hashiramoto, Hashimoto 648-0091, Japan

(*Received* 22 March 2004; *accepted* 19 August 2004)

Abstract – Mesoproterozoic supracrustal rocks in the Kibaride belt (southeast Congo) were intruded by mafic–intermediate plutonic rocks. These igneous rocks were affected by greenschist- to amphibolite-facies metamorphism during the Mesoproterozoic Kibaran orogenesis. U–Pb single zircon dating of the Mitwaba mafic–intermediate plutonic rocks yields an emplacement age of 1.38 Ga. The compositions of the Mitwaba mafic–intermediate plutonic rocks range from gabbro to diorite and show the following elemental concentrations: SiO_2: 49–58 wt %, TiO_2: 0.53–0.92 wt %, Al_2O_3: 13.1–18.68 wt %, Zr: 45–142 ppm, Y: 13–43 ppm. Mg no. 40–66 indicates variable degrees of fractionation of the magmas. The rocks are marked by high and variable Th/Ta (3–14), La/Nb (2–5) and low Ce/Pb (0.3–12.8) and Ti/V (10–19). Chondrite-normalized REE patterns exhibit enrichment in LREE relative to HREE ($(La/Yb)_N = 2.9–5.8$). Primordial mantle-normalized spider diagrams show negative slopes with gradual decrease from LIL to HFS elements and are marked by Nb and Ti negative anomalies. Immobile trace-element contents indicate a continental arc setting for these mafic–intermediate igneous rocks. They are inferred to have originated from a mantle wedge enriched by fluid from a subducting slab, with possibly an additional contribution from subducted sediments. Low, sub-chondritic Nb/Ta ratios in these mafic rocks support this interpretation. A model involving underplating of mafic–intermediate arc magma into the crust, triggering partial melting of Mitwaba group metasedimentary rocks during the accretionary stage of the Kibaran orogeny, is proposed to explain the coeval emplacement of mafic–intermediate arc magmas and peraluminous S-type granitoids in the Kibaride belt of central Africa.

Keywords: mafic–intermediate rocks, subduction, underplating, Kibaran Orogeny.

1. Introduction

The Mesoproterozoic Kibaran orogenic system of eastern central Africa is a linear belt stretching NE–SW from Katanga in Democratic Republic of Congo, hereafter Congo (Kibaride belt), through Burundi, eastern Congo, Rwanda (Burundian belt), Uganda, Tanzania (Karagwe–Ankolean belt) and northern Congo (Luhule–Mobisio) where it swings to a NW–SE direction (e.g. Kampunzu *et al*. 1986). This belt is among the least-studied Mesoproterozoic belts in the world, and despite its importance for Rodinia supercontinent reconstruction, its geotectonic evolution is as yet poorly constrained.

In eastern central Africa, the Kibaran belt is characterized by the emplacement of a huge amount of strongly peraluminous granitoids at *c*. 1.38 Ga (Kokonyangi *et al*. 2004*a*) and tin granites at *c*. 1.0–0.95 Ga (Cahen *et al*. 1984; Ikingura *et al*. 1992; Romer & Lehmann, 1995). The 1.38 Ga granitoids are spatially and temporally associated with mafic–intermediate plutonic rocks (e.g. Ntungicimpaye & Kampunzu, 1987; Deblond *et al*. 2001; Evans *et al*. 2000; Kokonyangi *et al*. 2004*a*). ^{40}Ar–^{39}Ar dating of Mesoproterozoic mafic rocks in the external portion of the northern Kibaran belt in Burundi and Tanzania yielded cooling ages between 1379 ± 10 and 1350 ± 10 Ma (Deblond *et al*. 2001). These ages are close to the SHRIMP U–Pb zircon crystallization age of widespread 1.37 Ga (error not given) synorogenic granitoids and subordinate mafic plutonic rocks documented in Burundi within the western internal domain of the northern Kibaran belt (e.g. Tack *et al*. 2002).

The present paper reports the results of investigations of mafic–intermediate plutonic rocks closely associated with 1.38 Ga Kibaran strongly peraluminous granitoids in the Mitwaba area (the type area for the Kibaran orogenic belt). The objectives of this study are as follows: (1) describe the field relationships between mafic–intermediate plutonic rocks and early Kibaran, strongly peraluminous granitoids and their

† Author for correspondence: joseph@sci.osaka-cu.ac.jp

https://doi.org/10.1017/S0016756804009951 Published online by Cambridge University Press

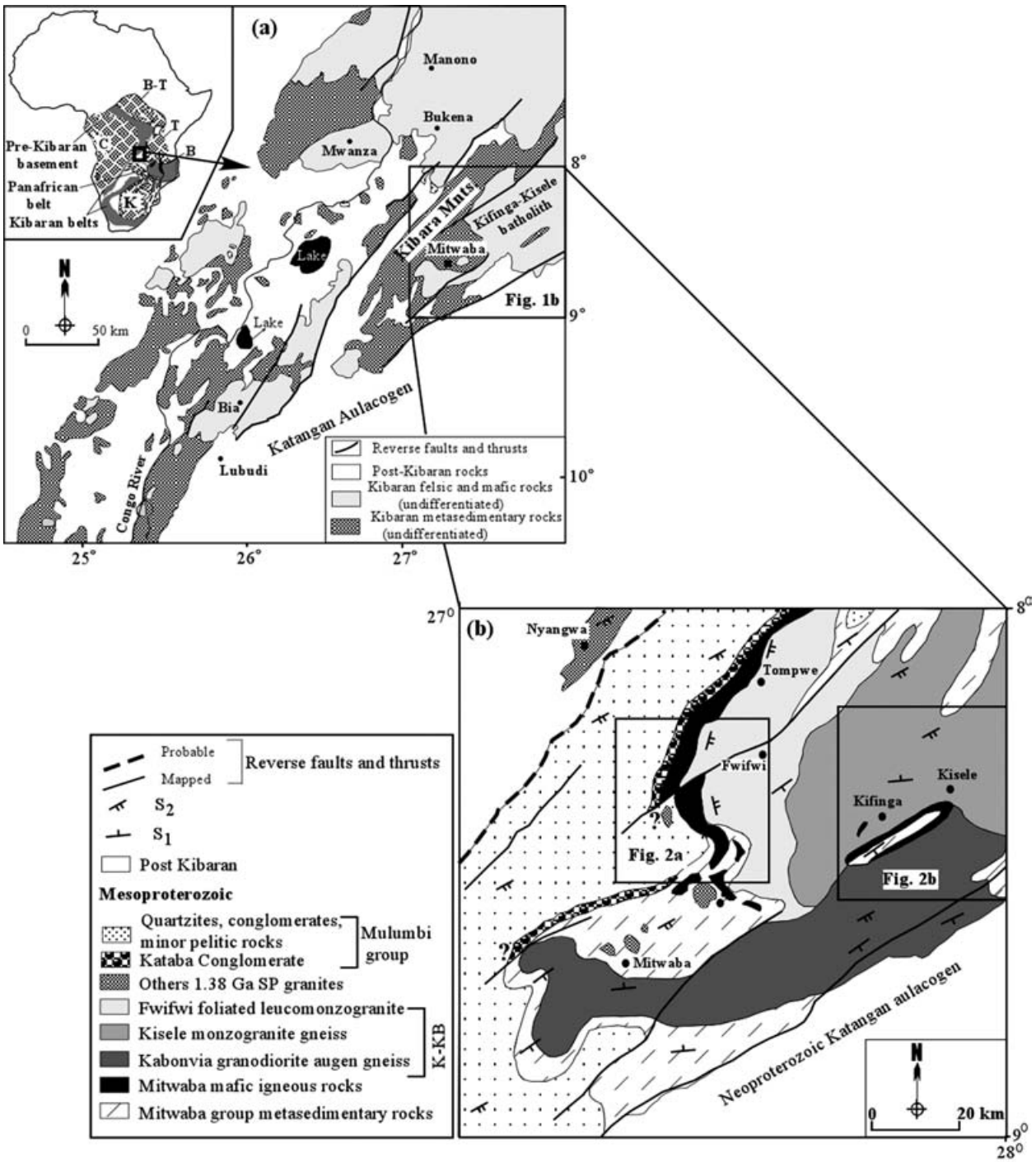

Figure 1. (a) Sketch map of the Kibaride belt (Katanga, D.R. Congo) showing the distribution of Mesoproterozoic metasedimentary and felsic and mafic igneous rocks. The upper left inset shows the position of the Kibaran orogenic system relative to the Congo (C), Buganda-Toro (B-T), Tanzania (T), Bangweulu (B) and Kalahari (K) Cratons. Modified after Cahen, Delhal & Deutsch (1967). (b) Geological map of the Mitwaba area showing the distribution of Kibaran mafic–intermediate plutonic rocks and spatially associated, strongly peraluminous 1.38 Ga granitoids. K-KB – Kifinga-Kisele batholith. Boxes show the locations of Figure 2a, b.

host metasedimentary rocks in the Mitwaba area; (2) constrain the emplacement age of the mafic–intermediate plutonic rocks using the U–Pb single zircon technique; (3) interpret the tectonic setting during the emplacement of the mafic–intermediate plutonic rocks and assess its implications for the evolution of the Kibaride belt.

2. Geological setting

The Kibaride belt of Katanga (Congo) represents the type-area of the Kibaran orogenic system of Africa (Cahen, 1954; Cahen *et al*. 1984; Kampunzu *et al*. 1986). It is a NE-trending linear belt (Fig. 1) extending over 600 km, with a width between 100 and 300 km. It

https://doi.org/10.1017/S0016756804009951 Published online by Cambridge University Press

is bounded to the east by a mosaic of continental blocks assembled before the Kibaran orogeny, including the Archaean Tanzania craton, and the Palaeoproterozoic Bangweulu block. To the west, the Kibaride belt is limited by the Archaean to Palaeoproterozoic Kasai–Congo Craton (Fig. 1). There is no geological correlation between pre-Mesoproterozoic terrains exposed on both sides of the Kibaride belt. Undeformed and unmetamorphosed Neoproterozoic Katangan sedimentary rocks unconformably overlie the Kibaride belt to the southeast of Mitwaba.

The Kibaride belt is composed of supracrustal metasedimentary rocks and a large quantity of granitic bodies (e.g. Cahen *et al*. 1984; Kampunzu *et al*. 1986; Kokonyangi *et al*. 2004*a*). The supracrustal metasedimentary rocks exposed in the Kibaride belt (> 10 km thick: e.g. Cahen *et al*. 1984) consist mainly of paragneisses, metapelites, siltstones, quartzites, conglomerates and minor carbonates. The sedimentary sequences were intruded by early Kibaran granitoids at 1381 ± 8 Ma (Kokonyangi *et al*. 2004*a*). Two informal lithostratigraphic groups were defined in the Mitwaba area: the older Mitwaba and the younger Mulumbi groups (Kokonyangi *et al*. 2001, 2004*a*). These two informal groups are separated by the Kataba Conglomerate (Cahen *et al*. 1984; Kokonyangi *et al*. 2001, 2004*b*). The Mitwaba group is made of gneisses, metapelites, calc-silicates, metamorphosed cherts and minor quartzites and volcano-sedimentary rocks. The Mulumbi group is composed of (1) the Kataba Conglomerate containing pebbles from the underlying Mitwaba group metasedimentary and (meta-)igneous rocks at the base; (2) quartzites and greywackes with several conglomerate intercalations; (3) slates and rare quartzite intercalations. The source terrains for the Kibaran sediments are as yet unknown but are inferred to consist predominantly of Palaeoproterozoic rocks, based on SHRIMP U–Pb data on detrital zircon studies in progress (Kokonyangi & Armstrong, unpub. data). The timing of deposition of the sedimentary rocks is also unknown. However, the older Mitwaba group is intruded by the 1381 ± 8 Ma granitoids, which do not cut the younger Mulumbi group. The latter group contains clasts from the underlying Mitwaba group granitoids and is intruded by the *c*. 1000 Ma tin granites (Kokonyangi *et al*. 2004*b*).

Two major deformation events (D_1 and D_2) affected the 1381 Ma Kibaran granitoids and their host Mitwaba group metasedimentary sequences (Kampunzu *et al*. 1986; Kokonyangi *et al*. 2001, 2004*a*, *b*). The earliest (D_1) is characterized by ENE-trending asymmetric folds and thrusts showing a N to NNW transport direction. These structures affect the metasedimentary rocks of the Mitwaba group and are not recorded within the Mulumbi group. D_2 is the main Kibaran deformation; it is characterized by macro- to mesoscopic isoclinal folds (F_2) and related axial cleavage (S_2). D_2 fabrics are well preserved in both the Mitwaba and Mulumbi groups. The Kataba Conglomerate at the base of the Mulumbi group was deposited after D_1 and the emplacement of syn-D_1 granites. The mineral parageneses defining the NE-trending S_2 foliation grew during Barrovian metamorphism and display an increase of metamorphic grade from the northwest (greenschist facies) to the southeast (amphibolite facies, Fig. 2a, b; Kokonyangi *et al*. 2001). Kampunzu *et al*. (1986, 1998) consider that the Kibaran deformation events mark the development of an active continental margin (~1.4–1.25 Ga) followed by a continental collision (~1.25–1.0 Ga), but there is no consensus on this interpretation (e.g. Klerkx *et al*. 1987). Kokonyangi *et al*. (2004*a*), using U–Pb SHRIMP zircon data from the Kisele orthogneiss (strongly deformed during D_2 and metamorphosed under amphibolite-facies metamorphism), constrained one continental collision event in the Mitwaba area of the Kibaride belt at 1079 ± 14 Ma.

3. Local geology

The distribution of mafic–intermediate plutonic rocks in the Mitwaba area is shown in Figures 1b and 2a–b. Geographically, these rocks are divided into the Lwabwe and Kidilo complexes. The Lwabwe mafic complex is a homogeneous, 1.5 to 3 km wide, arc-shaped metadolerite/metagabbro body forming a rim at the western margin of the Kifinga–Kisele batholith (Figs 1b, 2a). This granitic batholith includes the following individual plutons: Kabonvia granodioritic augen gneiss, Kisele monzogranite gneiss and Fwifwi foliated leucomonzogranite (Kokonyangi *et al*. 2004*a*). Magmatic zircons from the synkinematic D_1 Fwifwi foliated leucomonzogranite that is in contact with the Lwabwe plutonic mafic complex yielded a concordant U–Pb SHRIMP crystallization age of 1372 ± 9.6 Ma (Kokonyangi *et al*. 2004*a*). The Lwabwe plutonic mafic complex includes one main body wrapping the western margin of the Kifinga–Kisele batholith over 30 km and several subordinate discrete bodies covering 500 m^2 to 1 km^2 near Kakunko (e.g. Fig. 2a). The mafic complex intrudes into greenschist facies Mitwaba group metasedimentary rocks. The intrusive contact between the Lwabwe plutonic mafic complex and its host metasedimentary rocks of the Mitwaba group is exposed ~ 500 m west of Bulanda (Fig. 2a), where a sample from the chilled margin (Fig. 3a, c) was collected. The contact between the Kifinga–Kisele batholith and the Lwabwe plutonic mafic complex is often strongly sheared, although sharp intrusive contacts (for example, near Dibango and south of Komeshia; Fig. 2a) are exposed, showing that the Fwifwi foliated leucomonzogranite develops a chilled margin against, and contains angular enclaves of, the Lwabwe plutonic mafic complex. This mafic complex nowhere intrudes the Mulumbi group sedimentary units. Three hundred metres west of the Mwadianvula Falls (Fig. 2a), the mafic rocks are overlain by the Mulumbi group rocks, with the

https://doi.org/10.1017/S0016756804009951 Published online by Cambridge University Press

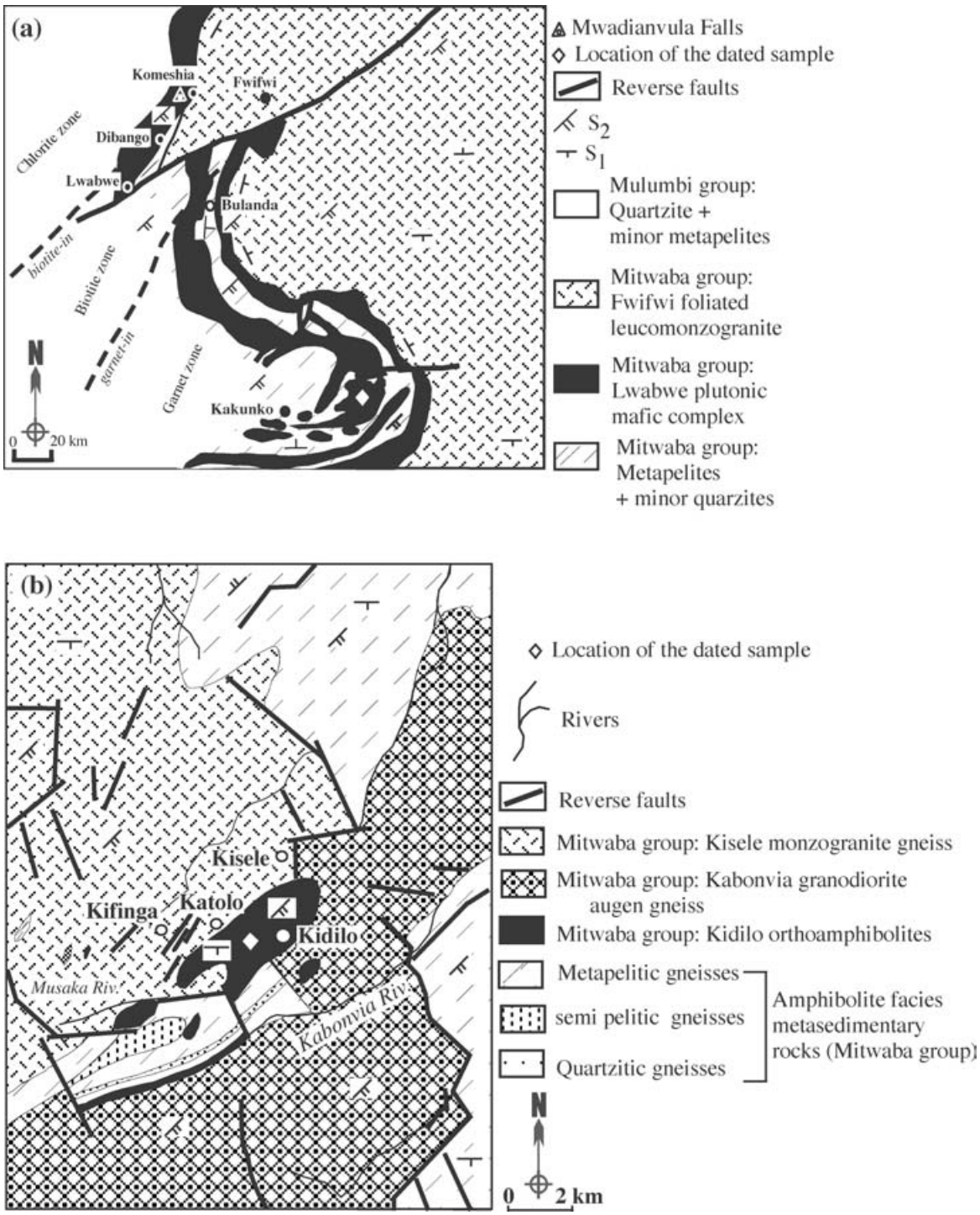

Figure 2. (a) Detailed geological map of the western margin of the Kifinga–Kisele batholith showing the relationship between the Lwabwe plutonic igneous complex and the Fwifwi foliated leucomonzogranite. The dashed lines show the metamorphic isograds (M_2) within the adjacent metasedimentary rocks (Kokonyangi *et al*. 2001). (b) Detailed geological map of south eastern Mitwaba area showing the occurrences of the Kidilo orthoamphibolite complex relative to the Kisele monzogranite gneiss, Kabonvia granodiorite augen gneiss and host metasedimentary rocks.

Kataba Conglomerate at the base of the later group (e.g. Fig. 1b). The mafic rocks and associated 1.38 Ga granitoids pre-date the deposition of the Mulumbi group sequences (Kokonyangi *et al*. 2001, 2004*b*). The Lwabwe plutonic mafic complex exhibits two foliations: a locally preserved relict S_1 defined by hornblende and plagioclase, and the regional S_2, which is defined by preferred orientation of biotite and actinolite and is parallel to S_2 in the host metasedimentary rocks. The modal quartz content in the Lwabwe metagabbro decreases from ~ 34 % near the contact with the granite (e.g. Fig. 3a) down to < 5 % about 60 m away of this

https://doi.org/10.1017/S0016756804009951 Published online by Cambridge University Press

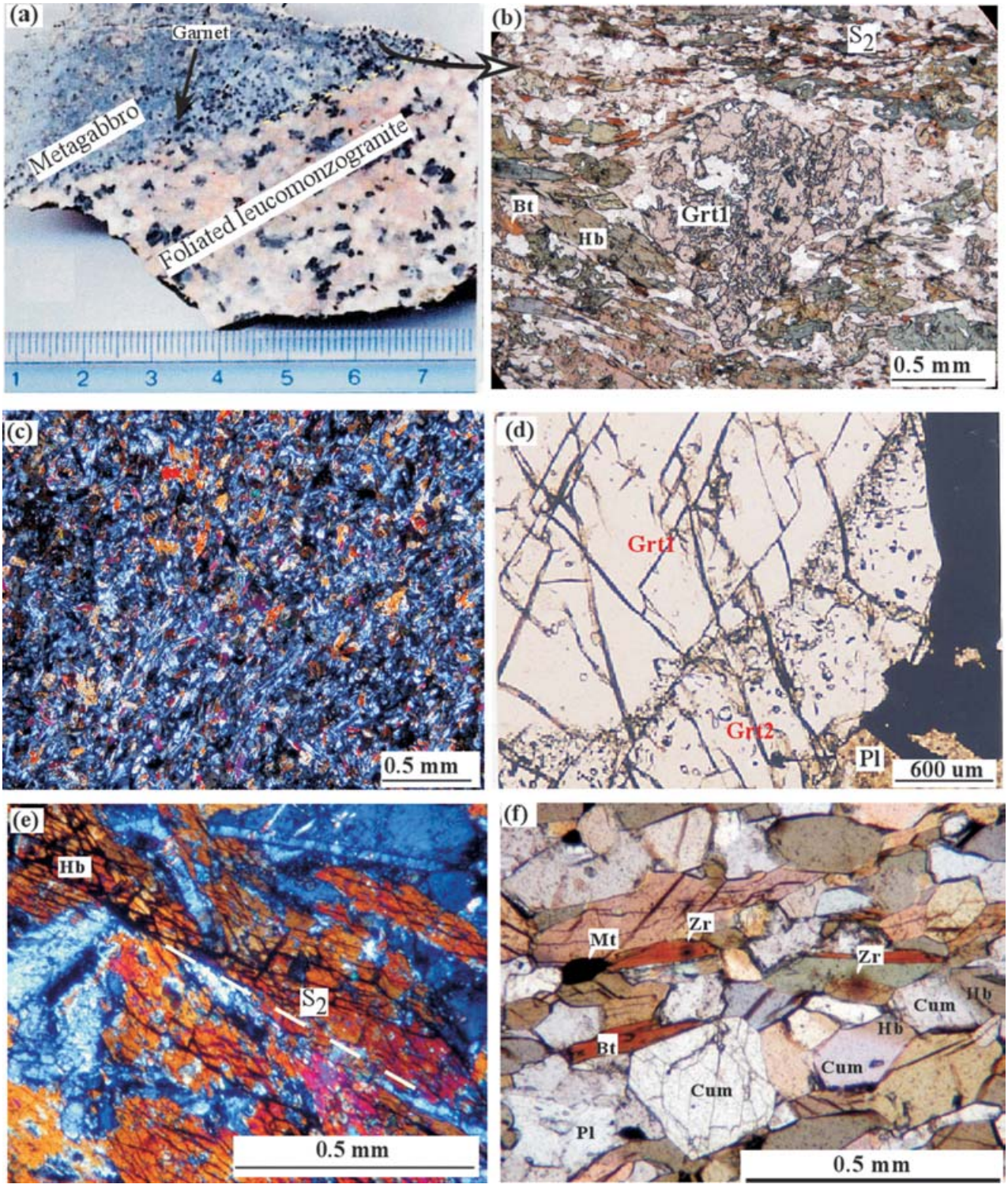

Figure 3. (a) Handspecimen photograph illustrating the contact between the Lwabwe metagabbro and the Fwifwi foliated leucomonzogranite near Dibango. (b) Photomicrograph from the sample in (a) collected < 5 m from the contact Lwabwe plutonic igneous complex and Fwifwi foliated leucomonzogranite. See text for explanation. (c) Photomicrograph of a sample collected from the contact between the Lwabwe plutonic igneous complex and Mitwaba group metasedimentary rocks at Bulanda. The mafic igneous rocks show a chilled margin against the host metasedimentary rocks of the Mitwaba group. (d) Garnet porphyroblast from the Kidilo orthoamphibolite complex collected < 10 m from the contact with the Kisele monzogranite gneiss. Note two different stages of garnet growth (Grt1–Grt2). (e) Microphotograph of the least deformed mafic rock sample from the Kidilo complex, showing preserved prismatic igneous hornblende and plagioclase laths. (f) Microphotograph showing the granoblastic texture in the Kidilo orthoamphibolites. S_1 is defined by preferred orientation of biotite and amphibole. Partial replacement of hornblende by cummingtonite illustrated in the lower right quarter of the photograph. Note the presence of a cummingtonite with a pyroxene-like shape. See text for details.

https://doi.org/10.1017/S0016756804009951 Published online by Cambridge University Press

contact, where the mafic body is not affected by silicification induced by fluids from the granite.

The orthoamphibolites of the Kidilo complex (Fig. 2b) are sandwiched between the Kisele monzogranite gneiss and the Kabonvia granodiorite augen gneiss, intruding metasedimentary rocks of the Mitwaba group (Fig. 2b). The rocks are black to dark-green, coarse- to medium-grained, and exposed within amphibolite-facies metamorphic rocks to the southeast of Mitwaba (Fig. 2b). The orthoamphibolites exhibit a strong S_2 foliation trending N15–30°E and defined by preferred orientation of amphiboles and biotite (Fig. 3f). The complex includes the main Kidilo orthoamphibolite body (*c*. 5 km long and 2 km wide) and four discrete subordinate bodies, such as the Kabonvia River orthoamphibolites forming a 100–200 m thick body extending over 3–4 km along the boundary between paragneisses and Kabonvia granodiorite orthogneiss (Fig. 2b). Igneous zircons yielded crystallization ages of 1386 ± 4.8 Ma and 1385 ± 7.4 Ma for the syn-D_1 Kisele monzogranite gneiss and Kabonvia granodiorite augen gneiss, respectively (Kokonyangi *et al*. 2004*a*). The intense D_1 and D_2 deformation fabrics along the orthoamphibolite-granitoids and orthoamphibolite–metasedimentary contacts preclude a detailed documentation of the original relationship between the Kidilo igneous complex and adjacent rocks. Angular xenoliths of the Kidilo orthoamphibolite in the Kisele monzogranite gneiss suggest that the igneous protolith of the amphibolite was emplaced before that of the orthogneiss.

No compositional zoning/layering was identified within the Lwabwe plutonic mafic complex or the Kidilo orthoamphibolite and associated discrete mafic bodies.

4. Sampling and analytical procedures

Fifty-one representative samples of mafic–intermediate plutonic rocks from Mitwaba were selected for geochemical investigation, ten samples for petrographic and microprobe analyses and two samples for U–Pb zircon geochronology. For the present study, highly deformed samples and those with veins and high contents of secondary minerals such as epidote, calcite and quartz were discarded. Samples used for geochemical investigations were massive and/or weakly foliated rocks collected far away from the contact with the granite and metasedimentary rocks.

Mineral compositions were obtained using an electron-probe microanalyser (Shimadzu EPMA-8705) housed at Osaka City University (Japan). The acceleration voltage was 15 kV, with a beam current of 4 nA and a beam diameter of 5 μm. Compositional mapping of garnet was performed using a wave-length dispersive electron probe microanalyser (JEOL JXA-8600M) at Kochi University (Japan), with an acceleration voltage of 15 kV, probe current of 7.5 nA, dwell time of 50 ms and beam diameter of 5 μm.

Samples selected for whole-rock chemical study were powdered using an automatic agate mill at Osaka City University (OCU), in order to avoid any contamination of metals such as Co, Ta and Nb. Two sets of new whole-rock chemical data are used in this paper. The first set includes twenty-six whole-rock analyses determined at OCU, using a Rigaku RIX-2000 X-ray fluorescence spectrometer on glass discs. These data correspond to the analyses without REE compositions in Table 2. The second set consists of twenty-five whole-rock analyses performed at ALS Chemex Laboratories (Canada). Major-element compositions were determined using an ICP-AES (detection limit 0.001 wt %), whereas trace elements were analysed using an ICP-MS (detection limits generally between 0.1 and 0.5 ppm). Pb, Ni, Cr and Li were analysed by AAS (detection limits 1 ppm). The precision for all the chemical analyses in this study is ± 1 % and ± 5 % for major and trace elements respectively. Samples from the same outcrop analysed at both Chemex and OCU show good agreement between results (within error).

Two samples, one from the Lwabwe complex (metagabbro LW507) and the other from the Kidilo complex (orthoamphibolite KM407) were selected for TIMS U–Pb zircon geochronology. Samples were prepared and analysed at Memorial University, Newfoundland, Canada. Rock samples were pulverized using a heavy-duty hydraulic rock splitter, jaw crusher and swing mill. Mineral separation involved the use of a Wilfley Table, heavy liquids (methylene iodide) and a Frantz Isodynamic Separator. Zircons were examined with a binocular microscope in order to assess grain quality, degree of fracturing and the possible existence of inherited cores. Handpicked zircons were abraded using the techniques of Krogh (1982) and washed in ultra-pure acetone and diluted nitric acid. Single grains or small populations of zircons were then placed into 0.35 ml Teflon vials together with 30 μl HF and a mixed ^{205}Pb–^{235}U spike. Eight of these Teflon vials were then placed in a Parr Container for four days at 220 °C. U and Pb were then chemically isolated by anion exchange columns, following the procedures described by Krogh (1973) but using smaller columns (0.05 ml of resin). The analyses were performed on an MAT262 mass spectrometer. A fractionation correction of 0.12 % per amu (± 0.05 %) was applied. Total Pb blanks over the period of the analyses range from 1.5 to 5 pg and a value of 5 pg was assigned as the laboratory blank ($^{206}Pb/^{204}Pb = 18.97 \pm 1$, $^{207}Pb/^{204}Pb = 15.73 \pm 0.5$ and $^{208}Pb/^{204}Pb = 39.19 \pm 1.5$). The calculation of common Pb was made by subtracting blanks and then assuming that the remaining common Pb has been incorporated into the crystal and has a composition determined from the model of Stacey & Kramers (1975). Data were reduced using PbDat (Ludwig, 1993). Analytical uncertainties are listed at 2σ and

https://doi.org/10.1017/S0016756804009951 Published online by Cambridge University Press

age determinations were processed using Isoplot/Ex (Ludwig, 2000).

5. Petrography and mineral chemistry

5.a. Lwabwe plutonic mafic complex

The Lwabwe plutonic mafic complex consists of dark greyish to greenish metadolerite–metagabbro, showing intergranular textures. The rocks mainly consist of prismatic igneous hornblende and plagioclase laths (e.g. Fig. 3e). Subordinate igneous and metamorphic minerals are biotite, quartz, titanite, zircon, apatite, opaque minerals, actinolite, chlorite, zoisite and minor carbonate. Primary prismatic hornblende contains zircon inclusions with strong pleochroic haloes. Igneous textures are locally preserved in the least deformed greenschist-facies rocks and are characterized by intergrowth between prismatic hornblende (0.3–1 mm long) and elongate laths of plagioclase (up to 0.5 mm long, e.g. Fig. 3e). There is no variation of mineral composition or modal proportion within the Lwabwe plutonic mafic complex. The mineral assemblage including actinolite–chlorite–epidote is diagnostic of greenschist-facies metamorphism (e.g. Yardley, 1989). However, within 10 m of the contact with the granite, the Lwabwe mafic complex has undergone contact metamorphism leading to the growth of porphyroblastic biotite and garnet (Fig. 3a, b). Biotite within the contact aureole is free of zircon inclusions. Within this contact aureole, the regional foliation (S_2) defined by preferred orientation of biotite and hornblende swings around garnet porphyroblasts (e.g. Fig. 3b). Locally (e.g. East of Bulanda, Fig. 2a), garnet porphyroblasts exhibit rounded cores free of inclusions and rims clouded with inclusions (quartz and opaques), producing euhedral to subhedral grains (Fig. 3d). The porphyroblast cores possibly grew during contact metamorphism (M_1) induced by the emplacement of syn-D_1 Fwifwi foliated leucomonzogranite (Kokonyangi *et al*. 2004*a*), whereas the rims are inferred to have grown during regional metamorphism (M_2). Samples collected from the Lwabwe plutonic mafic complex at its contact with the Mitwaba group metasedimentary rocks are fine-grained metadoleritic rocks composed of 0.03–0.09 mm long igneous plagioclase and 0.05–0.2 mm long hornblende. This fine-grained lithology represents a chilled margin against the Mitwaba group metasedimentary country rocks (e.g. Fig. 3c).

Representative chemical analyses of the main rock forming minerals of the Lwabwe plutonic mafic complex are given in Table 1 and plotted in Figure 4a–b. Two types of plagioclase and hornblende can be distinguished. Away from the contact with the granite (>30 m), relict euhedral magmatic labradorites (An up to 66, Fig. 4a) are common. The main amphibole is a metamorphic actinolite ($X_{Mg} = (Mg/Mg + Fe^{2+}) =$ 0.71–0.76), although some relict euhedral magnesio-hornblende ($X_{Mg} \sim 0.52$) was noticed (Table 1; Fig. 4b). Hornblende crystals rimmed by actinolite/actinolitic hornblende record retrograde transformation of igneous amphibole. Close to the contact with the granite (<15 m), plagioclase is andesine ($An_{30–44}$) and amphibole is ferro-tschermakite ($X_{Mg} = 0.39–0.43$; Table 1, Fig. 4a, b). Chemical mapping of garnet porphyroblasts shows uniform Ca-poor and Fe-rich cores, surrounded by rims displaying reverse zoning (Table 1). Most cores have embayed margins indicating partial resorption, a common feature of polymetamorphic garnets (e.g. Barker, 1998).

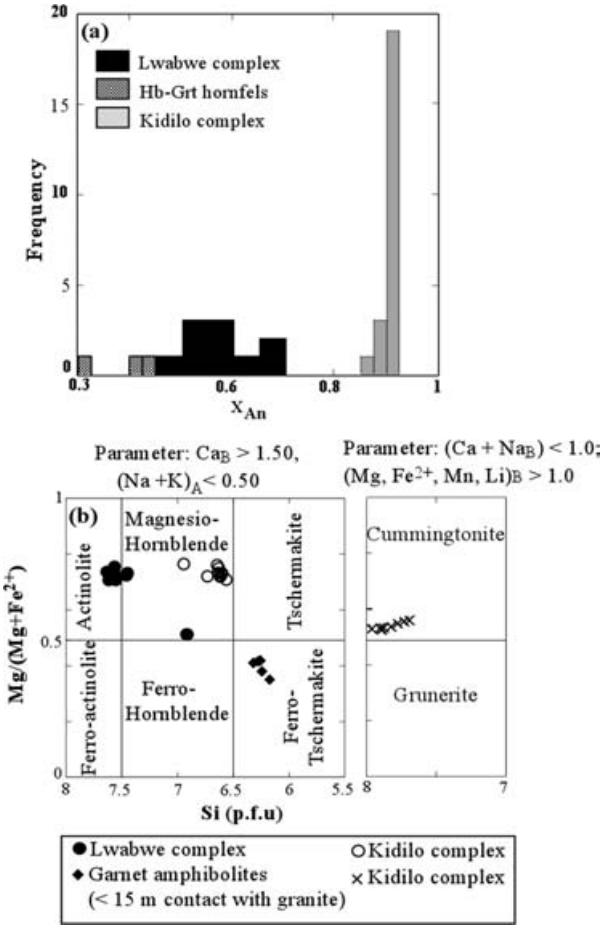

Figure 4. Diagrams of representative mineral compositions of Mitwaba mafic–intermediate plutonic rocks: (a) plagioclase; (b) amphiboles (plotting parameters are after Leake *et al*. 1997). See text for details.

5.b. Kidilo orthoamphibolite complex

The samples from Kidilo display granoblastic texture (Fig. 3f). The Kidilo orthoamphibolite is mainly composed of hornblende (0.2–0.8 mm) and plagioclase (0.25–0.5 mm), cummingtonite, biotite and quartz, with rare relict igneous orthopyroxene (0.25–0.40 mm, Table 1). The main accessories are zircon and magnetite (Fig. 3f). Magnetite exhibits sharp contacts with zircon. The main amphiboles are magnesio-hornblende

https://doi.org/10.1017/S0016756804009951 Published online by Cambridge University Press

https://doi.org/10.1017/S0016756804009951 Published online by Cambridge University Press

Table 1. Representative mineral compositions of Mitwaba mafic to intermediate rocks

	Plagioclase													Grt			
	LM1	LM2	LM3	LM4	cont. 1	cont. 2	cont. 3	KM1	KM2	KM3	KM4	KM5	Opx	Bt	Core	Rim	Ilm	Mag
SiO_2	53.16	53.76	56.35	50.49	57.93	58.81	58.39	57.95	43.75	44.10	44.42	43.81	57.66	36.09	37.50	37.85	0.00	0.09
TiO_2	0.05	0.00	0.03	0.01	0.01	0.01	0.00	0.02	0.00	0.02	0.00	0.00	0.00	1.77	0.10	0.42	53.97	0.00
Al_2O_3	29.47	30.40	28.89	31.14	25.04	24.50	25.95	27.44	37.53	37.63	37.65	38.19	1.42	17.78	20.76	20.88	0.04	0.00
FeO	0.60	0.17	0.01	0.13	0.82	3.58	0.38	0.12	0.14	0.00	0.22	0.13	20.67	18.24	21.54	19.44	46.58	79.58
MnO	0.00	0.07	0.00	0.00	0.08	0.02	0.01	0.00	0.00	0.00	0.00	0.00	0.38	0.15	12.20	12.23	0.94	0.00
MgO	0.09	0.00	0.00	0.11	0.07	0.27	0.01	0.00	0.00	0.00	0.00	0.00	17.41	11.64	0.91	0.91	0.12	0.00
CaO	11.40	11.38	9.38	13.53	8.83	6.02	8.43	8.26	17.60	17.40	17.03	17.16	0.57	0.00	6.97	8.24	0.16	0.06
Na_2O	4.72	4.85	6.00	3.68	6.03	6.43	6.31	7.00	0.94	0.93	1.03	1.10	1.00	0.00	0.03	0.00	0.04	0.03
K_2O	0.22	0.06	0.07	0.13	0.40	0.76	0.24	0.06	0.03	0.00	0.01	0.00	0.00	10.84	0.00	0.00	0.02	0.01
Total	99.72	100.68	100.73	99.20	99.20	100.41	99.73	100.85	99.99	100.09	100.36	100.39	99.12	96.50	100.00	99.96	101.80	79.76
An	0.56	0.56	0.46	0.67	0.44	0.32	0.42	0.39	0.91	0.91	0.90	0.90						
Ab	0.42	0.43	0.53	0.33	0.54	0.63	0.57	0.60	0.09	0.09	0.10	0.10						
Or	0.01	0.00	0.00	0.01	0.02	0.05	0.01	0.00	0.00	0.00	0.00	0.00						

	Amphiboles																	
	LM1	LM2	LM3	LM4	LM5	cont. 1	cont. 2	cont. 3	cont. 4	KM1	KM2	KM3	KM4	KM5	KM6	KM7	KM8	KM9
SiO_2	53.43	52.91	51.17	52.32	46.33	41.90	41.65	41.44	41.32	45.60	47.61	46.42	45.77	53.25	53.63	54.09	53.22	53.89
TiO_2	0.06	0.24	0.17	0.06	0.31	0.25	0.36	0.45	0.28	0.57	0.46	0.66	0.66	0.01	0.02	0.01	0.00	0.08
Al_2O_3	2.54	3.24	3.88	3.89	10.15	15.78	15.52	15.66	16.33	11.90	11.28	11.67	12.11	0.70	0.63	0.66	0.67	0.69
FeO	11.94	12.80	12.84	12.66	16.41	18.56	17.68	17.71	18.40	15.15	15.03	15.03	14.56	24.92	25.34	24.71	24.70	25.63
MnO	0.17	0.29	0.34	0.41	0.72	0.81	0.65	0.64	0.66	0.18	0.28	0.25	0.16	0.73	0.65	0.70	0.58	0.59
MgO	16.32	15.30	14.97	14.75	9.43	6.59	6.68	6.58	6.22	11.07	11.89	11.71	11.32	16.38	16.66	16.50	16.51	16.84
CaO	13.14	12.02	12.47	12.33	12.20	11.99	11.96	11.91	12.19	10.89	11.27	11.07	11.08	0.87	0.75	0.71	0.84	0.84
Na_2O	0.20	0.27	0.33	0.35	0.95	1.30	1.24	1.05	1.18	0.80	0.86	0.76	0.82	0.04	0.06	0.05	0.02	0.05
K_2O	0.14	0.09	0.13	0.11	0.08	0.22	0.30	0.53	0.59	0.20	0.23	0.25	0.22	0.02	0.00	0.00	0.00	0.00
Total	97.95	97.16	96.20	96.88	96.57	97.41	96.04	95.97	97.17	96.35	98.90	97.81	96.69	96.91	97.73	97.44	96.54	98.60
Al^{IV}	0.36	0.42	0.54	0.42	1.068	1.73	1.66	1.71	1.74	1.37	1.26	1.36	1.37	0.08	0.09	0.03	0.07	0.11
Al^{VI}	0.07	0.13	0.13	0.24	0.721	1.06	1.12	1.09	1.17	0.67	0.62	0.60	0.70	0.05	0.02	0.09	0.05	0.00
Fe^{3+}	0.17	0.49	0.41	0.23	0.076	0.34	0.12	0.22	0.11	0.92	0.83	0.99	0.83	0.00	0.07	0.00	0.02	0.09
Fe^{2+}	1.26	1.04	1.16	1.30	1.974	1.98	2.13	2.02	2.22	0.92	0.95	0.81	0.94	3.10	3.06	3.05	3.06	3.04
X_{Mg}	0.74	0.76	0.74	0.71	0.516	0.43	0.42	0.42	0.39	0.72	0.73	0.76	0.72	0.54	0.55	0.54	0.55	0.55
$(Ca+Na)_B$	2.01	1.92	2.00	2.00	2.00	2.00	2.00	2.00	2.00	1.92	1.95	1.91	1.95	0.14	0.13	0.12	0.14	0.15
$(Na+K)_A$	0.08	0.02	0.06	0.03	0.25	0.35	0.37	0.34	0.43	0.04	0.04	0.04	0.04	0.00	0.00	0.00	0.00	0.00
Na_B	0.00	0.08	0.06	0.09	0.05	0.08	0.05	0.07	0.03	0.23	0.24	0.22	0.24	0.01	0.02	0.01	0.01	0.02

LM – Lwabwe plutonic mafic complex (greenschist); KM – Kidilo orthoamphibolite complex; cont. – minerals from the contact aureole; Ilm – Ilmenite (sample LM); Grt – Garnet; Opx – Orthopyroxene (sample KM), Mag – Magnetite (sample KM); Bt – Biotite (sample LM); Garnet analyses are from grain shown in Figure 3d.

($X_{Mg} = 0.72–0.77$), cummingtonite ($X_{Mg} = 0.54–0.55$), and the plagioclase is bytownite ($An_{86–90}$) (Table 1, Fig. 4a, b). In most samples of the Kidilo orthoamphibolite complex, textural evidence suggests partial replacement of pyroxene and/or hornblende by cummingtonite, as shown by cummingtonite with pyroxene-like shapes (Fig. 3f), and by hornblende grains showing embayed margins against adjacent cummingtonite. The above data and the presence of Ca-rich plagioclase (up to An90) suggest growth of cummingtonite during metamorphic recrystallization according to the following reactions:

$$\underset{\text{orthopyroxene}}{7(Mg, Fe)SiO_3} + H_2O + SiO_2 = \underset{\text{cummingtonite}}{(Mg, Fe)_7Si_8O_{22}(OH)_2} \quad (1)$$

$$\underset{\text{hornblende}}{7Ca_2(Mg, Fe)_3Al_4Si_6O_{22}(OH)_2} + 10SiO_2 = \underset{\text{cummingtonite}}{3(Mg, Fe)_7Si_8O_{22}(OH)_2} + \underset{\text{anorthite}}{14CaAl_2Si_2O_8} + 4H_2O \quad (2)$$

Biotite flakes cut across or partially replace hornblende. Zircon inclusions are rimmed by strong pleochroic haloes in hornblende and biotite (Fig. 3f). Other accessory minerals include quartz, apatite and ilmenite (Table 1). The presence of hornblende–(cummingtonite)–plagioclase and the absence of actinolite–chlorite–epidote suggest amphibolite-facies conditions during metamorphic recrystallization (e.g. Yardley, 1989; Spear, 1993).

6. Whole rock geochemistry

6.a. Element mobility

Geochemical characteristics of Precambrian igneous rocks provide important constraints for the geotectonic setting at the time of magma emplacement (e.g. Polat, Kerrich & Wyman, 1998; Puchtel *et al*. 1998). However, element mobility is a major concern when studying igneous suites where primary textures and mineralogy have been overprinted by solid-state deformation and metamorphism.

The Mitwaba mafic–intermediate plutonic rocks have undergone greenschist to amphibolite-facies metamorphism. However, the distribution of strain in the study area is heterogeneous and the grade of metamorphism is variable (Kokonyangi *et al*. 2001). Therefore, element mobility can be tested by comparing the composition of rocks with igneous mineralogy and texture locally preserved in greenschist-facies metamorphic zones (e.g. samples LM, Fig. 3c, e, Table 2) with those highly deformed and metamorphosed in the amphibolite facies (samples KM, Fig. 3f, Table 2). Nb and Zr are incompatible elements, especially in mafic and intermediate igneous rocks, and are generally immobile during greenschist- to amphibolite-facies metamorphism (e.g. Ludden, Gelinas & Trudell, 1982). These two elements were plotted against major and other trace elements in order to assess element mobility during metamorphism (Fig. 5a–l). Table 2 shows that Na, K, Ca, Ba Rb and Sr exhibit variable concentrations in spite of a relatively restricted range in SiO_2. In Figure 5a–d, these elements show wide scatter and lower average contents in samples from the amphibolite facies Kidilo complex when compared to those from the greenschist-facies Lwabwe complex. These observations suggest that most of the Large Ion Lithophile elements (LILE) were mobilized during metamorphism, especially as the mobility of these elements is a well-known phenomenon in metamorphosed igneous rocks (e.g. Arndt, 1994 and references therein). Based on a large number of geochemical studies of metamorphosed igneous rocks, there is a broad consensus that the least mobile elements are Al, Ti, high field strength elements (HFSE: Th, Nb, Ta, Zr, Hf), rare earth elements (REEs, excluding Eu), Y, Sc and V (e.g. Ludden, Gelinas & Trudell, 1982; Arndt, 1983; Rollinson, 1993), although a few studies have shown that some of these elements can be mobilized during intense hydrothermal alteration and metamorphism involving carbonates (e.g. Munz, Wayne & Austrheim, 1994). Table 2 shows coherent geochemical contents for greenschist and amphibolite-facies samples in terms of Ti, Zr, Ta, Th, Nb, Y, REEs, Co, Cr, Ni, Fe_2O_3, MgO, and these elements typically display systematic linear trends against Zr and Nb in Figure 5e–l, supporting their relative immobility. The relative immobility of the HFSE is also supported by parallel patterns between samples in normalized multi-element diagrams (see Section 5.b). In Figure 5h, although the data show scatter, this cannot be attributed to metamorphism because it is of the same magnitude in greenschist- and amphibolite-facies samples, and the Pb concentrations are similar to those reported in modern unmetamorphosed mafic rocks (e.g. Chauvel, Goldstein & Hofmann, 1995). This suggests that Pb was also relatively immobile.

The immobile elements discussed above will be used for classification, geochemical comparisons and interpretation of the geotectonic affinities of the Mitwaba mafic–intermediate plutonic rocks. Furthermore, the data were recalculated to 100 % anhydrous for inter-sample comparison (text and diagrams) to minimize the effects of secondary 'alteration'.

6.b. Major and trace element compositions

The rocks from the Kidilo orthoamphibolite complex are of intermediate composition, with SiO_2 in the range 54–58 wt %, whereas those from the Lwabwe plutonic mafic complex are of mafic–intermediate composition (SiO_2: 49–57 wt %). On the Zr/TiO_2 v. Nb/Y diagram of Winchester & Floyd (1977; Fig. 6a), the samples from both complexes plot at the boundary between andesite and andesite/basalt, suggesting that

https://doi.org/10.1017/S0016756804009951 Published online by Cambridge University Press

https://doi.org/10.1017/S0016756804009951 Published online by Cambridge University Press

Table 2. Representative major (wt %) and trace (ppm) element compositions of Mitwaba mafic to intermediate rocks

Sample no.	LM1	LM2	LM3	LM4	LM5	LM6	LM7	LM8	LM9	LM10	LM11	LM12	LM13	LM14	LM15	LM16	LM17	LM18	LM19	LM20	LM21
SiO_2	50.61	48.28	54.82	51.65	52.83	53.26	55.65	55.56	51.71	56.14	52.97	54.15	51.57	55.97	54.95	49.29	50.20	47.25	47.90	53.88	51.87
TiO_2	0.80	0.65	0.59	1.07	0.55	0.55	0.64	0.63	0.66	0.66	0.71	0.59	0.62	0.63	0.61	0.73	0.78	0.65	0.65	0.59	0.76
Al_2O_3	14.86	17.68	13.99	13.10	14.11	14.25	14.46	14.48	15.03	13.75	13.07	14.02	14.55	13.92	14.23	15.24	16.36	17.78	18.04	14.27	13.57
Fe_2O_3	10.62	9.48	9.01	14.65	8.39	8.44	8.82	8.88	8.69	8.88	11.39	9.65	8.93	9.17	9.79	11.1	11.01	9.61	9.67	9.15	15.18
MnO	0.19	0.22	0.16	0.20	0.21	0.21	0.22	0.22	0.10	0.15	0.2	0.24	0.1	0.15	0.24	0.21	0.20	0.23	0.23	0.17	0.21
MgO	7.37	6.73	6.78	5.93	7.22	7.24	5.83	5.82	8.31	5.80	8.63	6.43	8.73	5.92	6.46	7.91	7.68	6.76	6.87	7.03	5.19
CaO	10.55	8.73	9.40	8.82	9.04	9.17	7.59	7.59	9.57	10.55	9.7	7.75	9.11	10.12	7.68	10.64	10.71	8.61	8.71	9.41	8.95
Na_2O	0.84	1.90	1.78	2.36	2.73	2.75	2.41	2.41	1.81	1.66	0.97	2.4	1.89	1.69	2.47	0.83	0.83	1.90	1.96	1.77	2.47
K_2O	0.22	2.49	1.58	1.39	1.69	1.64	1.69	1.66	1.26	0.89	0.72	1.12	1.23	1.08	1.38	0.2	0.13	2.40	2.43	1.49	1.30
P_2O_5	0.07	0.04	0.06	0.19	0.05	0.03	0.04	0.06	0.07	0.05	0.13	0.08	0.12	0.16	0.12	0.11	0.07	0.04	0.05	0.05	0.21
LOI	2.91	3.27	2.47	0.28	2.64	2.59	2.01	2.18	2.95	0.90	1.59	2.07	2.71	0.85	1.94	2.62	2.46	3.60	1.62	0.43	0.21
Total	99.04	99.47	100.64	99.64	99.46	100.13	99.36	99.49	100.16	99.43	100.1	98.59	99.63	99.74	99.96	98.93	100.44	98.83	98.12	98.23	99.91
Mg no.	58	58	60	44	63	63	57	56	65	56	57	54	64	54	55	56	58	58	58	60	40
Ba	42.5	634	291	323	266	228	420	413	92	185.5	77.74	248.5	89.79	187.23	298.9	38.61	49	592	587	292	292
Cr	288	376	470	74	518	530	342	344	496	434	367.03	420.56	541.46	459.19	423.77	373.71	285	394	398	494	74
Cu	25	10	5	185	15	15	5	5	15	10	22.26	5.53	16.59	18.01	9.77	14.96	12	4	6	1	159
Nb	7.02	5.3	5	10	3	3.13	5	6	4	5.33	6.33	5.18	4.08	5.39	5.2	6.76	8	6.08	6.18	6.38	10
Ta	1.5	1.5	2	1.5	0.5	0.5	0.5	2	0.5	1	0.65	0.62	0.51	0.85	0.66	0.54					
Ni	40	5	5	65	10	5	5	5	65	5	41.47	6.67	70.2	7.89	24.97	40.75	36	6	7	9	59
Pb	7	10	7	4	7	7	6	7	2	3	5	3	3	3	5	6	11	9	9	8	2
Rb	6.8	173	65.4	75.6	92.6	83.2	95	94	84.8	44	50.82	62.37	80.3	50.39	72.67	6.63	6	154	156	63	63
Sr	174	207	125.5	175.5	173	151	190	186.5	90.5	149	80.3	195.51	94.56	151.91	189.91	75.09	163	200	203	130	164
V	280	230	220	265	245	230	205	210	235	225	292.81	219.25	230.34	218.2	218.15	290	252.9	216.3	217.4	217.9	241.1
Zr	86	95.5	85	133	73.5	59	95.5	97	63.5	101	72.88	92.64	66.44	100.46	98.63	77.09	90	104	105	93	142
Zn	125	90	75	140	85	85	80	85	90	85	102.38	93.3	50.73	73.25	87.4	128.69	122	88	88	76	119
Y	31.5	21.5	21	42.5	20.5	18.5	21	20.5	17.5	20.5	25.98	21.69	19.52	22.75	21.49	33.02	32	25	24	25	42
Th	4	6	5	6	4	3	6	6	3	6	4.34	6.77	4.46	7	6.71	4.8					
U	1	1.5	1.5	1	1	0.5	1.5	1.5	0.5	1.5	0.69	1.12	0.81	1.34	1.14	0.69					
Ce	30.5	37.5	30.5	48	30	26	33.5	33.5	23	35.5	25.42	35.61	25.52	38.39	34.85	34.64					
La	22.5	19	17	22	16	14	17	17	9	17.5	11.57	16.96	12.26	18.3	16.42	8.91					
Cs	1.7	10.1	3.1	7.8	3.4	2.8	7	7.1	6.7	2.5	8.74	5.98	6.9	3.25	5.92	1.48					
Sm	5.5	3.8	3.2	6.5	3.3	2.8	3.4	3.7	3	3.6	3.59	3.52	2.96	3.75	3.51	7.18					
Nd	24	18.5	15.5	26.5	15	13.5	16.5	15.5	22.1	17	14.06	16.01	12.19	17.66	15.75	31.78					
Er	3.9	2.3	2.5	4.8	2.2	2.1	2.3	2.4	2.1	2.4	2.52	2.19	2.02	2.21	2.21	3.4					
Eu	1.5	0.9	0.9	1.9	0.9	0.8	0.9	0.9	0.8	0.9	0.94	0.92	0.79	0.92	0.86	1.5					
Ga	18	19	16	24	17	15	17	17	17	17	14.99	15.17	14.84	15.1	15.14	16.16					
Gd	6.4	4.3	3.6	7.7	3.8	3.1	3.5	3.4	3.3	3.9	3.89	3.53	2.99	3.81	3.4	6.4					
Hf	2	2	2	5	1	1	3	3	1	2	2.26	2.93	2.2	3.19	3.09	2.46					
Ho	1.4	0.8	0.8	1.7	0.7	0.7	0.8	0.8	0.7	0.8	0.97	0.82	0.76	0.85	0.78	1.32					
Dy	6.4	4	3.7	8.1	4.3	3.1	3.8	3.8	2.9	3.8	4.01	3.26	3.03	3.54	3.35	5.65					
Lu	0.5	0.3	0.3	0.8	0.3	0.3	0.3	0.4	0.3	0.4	0.39	0.35	0.31	0.36	0.35	0.56					
Pr	6.1	4.5	3.8	6.2	3.8	3.2	4	4.2	3	4.3	3.3	4.32	3.1	4.58	4.21	8.34					
Tb	1	0.6	0.5	1.2	0.6	0.4	0.6	0.6	0.6	0.6	0.59	0.53	0.48	0.56	0.52	0.97					
Tm	0.6	0.3	0.3	0.7	0.3	0.3	0.3	0.3	0.3	0.3	0.39	0.35	0.31	0.36	0.35	0.55					
Yb	3.4	2.2	2.2	5	2.2	2.2	2.4	2.4	1.7	2.5	2.6	2.22	1.97	2.34	2.25	3.61					
Th/Ta	3	4	3	4	8	6	12	3	6	6	7	11	9	8	10	9					
Nb/Ta	5	4	3	7	6	6	10	3	8	5	10	8	8	6	8	13					
La/Nb	3	4	3	2	5	4	3	3	2	3	2	3	3	3	3	4					
Th/Ce	0.13	0.16	0.16	0.13	0.13	0.12	0.18	0.18	0.13	0.17	0.17	0.19	0.17	0.18	0.19	0.14					
Ce/Pb	4.4	3.8	4.4	12.0	4.3	3.7	5.6	4.8	11.5	11.8	5.1	11.9	8.5	12.8	7.0	5.8					
$(La/Yb)_{cn}$	4.4	5.8	5.2	2.9	4.9	4.3	4.7	4.7	4.7	4.7	3.0	5.1	4.2	5.2	4.9	5.4					

https://doi.org/10.1017/S0016756804009951 Published online by Cambridge University Press

Table 2. (continued)

Sample no.	LM22	LM24	LM25	LM26	LM27	LM28	LM31	LM32	KM1	KM3	KM4	KM5	KM6	KM7	KM8	KM9	KM10	KM11	KM12	KM14	KM15	KM17	KM18	KM19
SiO_2	52.52	55.24	55.39	51.20	48.97	49.19	50.75	50.73	54.15	52.48	53.2	53.99	52.31	52.69	54.74	55.78	52.39	52.25	52.46	53.30	53.42	52.49	51.08	52.62
TiO_2	0.55	0.64	0.67	0.67	0.64	0.77	0.65	0.65	0.76	0.69	0.7	0.77	0.52	0.70	0.82	0.62	0.69	0.73	0.74	0.84	0.82	0.72	0.67	0.72
Al_2O_3	14.74	15.00	14.36	15.27	14.62	15.58	15.35	15.32	14.45	14.59	14.69	14.17	14.64	14.39	14.42	14.42	14.86	14.81	14.95	14.50	14.77	14.74	15.24	14.79
Fe_2O_3	8.63	9.16	9.19	8.92	8.39	11.29	8.74	8.83	11.05	10.12	10.29	9.42	9.31	9.05	10.99	9.23	9.37	10.40	10.35	10.86	11.28	10.34	8.90	10.31
MnO	0.22	0.23	0.15	0.10	0.10	0.21	0.10	0.10	0.18	0.18	0.18	0.22	0.17	0.15	0.17	0.15	0.17	0.18	0.02	0.21	0.18	0.26	0.10	0.26
MgO	7.59	6.09	6.06	8.72	8.28	7.92	8.45	8.56	7.2	7.47	7.6	6.03	8.14	7.42	7.03	6.1	7.72	7.51	7.48	7.64	7.73	8.05	8.61	7.97
CaO	9.18	7.66	10.67	9.59	9.15	10.94	9.53	9.50	9.91	9.69	9.82	5.81	11.58	10.58	10.03	10.26	10.69	9.87	9.91	5.79	10.05	10.32	9.56	10.38
Na_2O	2.86	2.54	1.70	1.85	1.81	0.79	1.98	1.92	0.78	1.04	1.04	0.76	0.92	0.80	0.79	1.63	0.80	1.01	1.00	0.71	0.74	0.63	1.87	0.67
K_2O	1.63	1.61	0.86	1.21	1.16	0.12	1.23	1.24	0.27	0.84	0.81	2.95	0.12	0.96	0.29	0.99	0.88	0.76	0.74	2.85	0.20	0.13	1.20	0.12
P_2O_5	0.04	0.05	0.06	0.05	0.05	0.07	0.04	0.05	0.19	0.11	0.14	0.11	0.14	0.05	0.06	0.11	0.05	0.06	0.01	0.08	0.07	0.05	0.05	0.05
LOI	1.03	1.05	0.37	1.65	3.20	2.06	2.47	1.06	0.39	1.27	1.3	3.64	0.51	1.52	0.57	0.64	1.10	2.22	0.87	1.33	0.43	1.46	0.96	2.11
Total	98.98	99.26	99.48	99.22	96.35	98.92	99.29	97.95	99.36	98.51	99.81	97.87	98.38	98.31	99.91	100	98.69	99.80	98.53	98.11	99.67	99.19	98.24	100
Mg no.	64	57	57	66	66	58	66	63	54	57	57	53	61	62	56	54	62	59	59	58	58	58	66	58
Ba	233	401	175	104	97	46	101	105	19.81	98.04	96.96	190.19	28.24	60	23	196	63	102	102	190	27	13	94	19
Cr	561	349	419	490	457	312	470	477	268.12	317.55	313.02	248.31	201.5	354	228	440	369	261	263	190	225	484	486	475
Cu	9	1	4	16	14	10	9	9	19.97	26.99	27.56	18.93	8.86	25	20	5	15	20	18	13	10	2	9	4
Nb	4.05	6.21	6	5.32	4	6.23	5.11	5.09	7.63	6.47	6.52	7.77	2.98	5	7	6	5	7	6	8	7	4	5	5
Ta									0.74	0.61	0.59	0.64	0.5	1.5	1.5	0.5								
Ni	5	2	4	62	59	36	61	63	28.59	36.26	34.93	29.88	17.32	25	25	5	19	31	32	19	22	50	62	56
Pb	8	7	2	3	1	13	2	2	4	6	6	3	58	5	3	4	3	5	5	2	2	12	1	10
Rb	79	88	42	83	77	5	86	85	10.97	64.76	62.3	128.93	9.27	96	12.2	51.4	77	62	61	126	7	11	82	32
Sr	159	190	155	97	91	167	101	99	124.17	104.62	106.75	101.63	166.6	130	115	164.5	118	100	102	98	119	133	97	135
V	226.1	207.5	211	227.6	212.5	281.9	247.1	246.8	294.61	275.56	265.26	304.44	304.1	320	260	230	261.1	266.6	262.5	278.7	278.3	288.2	227.6	289
Zr	66	108	113	74	70	88	75	74	84.97	73.12	71.6	88.93	54.12	80.5	78.5	102	82	81	82	95	93	77	75	78
Zn	80	85	71	30	29	123	29	30	50.59	102.54	96.21	62.06	194.29	70	45	65	60	93	93	51	41	199	30	197
Y	22	24	24	21	21	33	21	21	25.37	22.63	22.58	26.05	14.15	21	22.5	22.5	22	24	24	28	26	22	20	22
Th									5.63	4.37	4.08	5.16	2.93	4.12	4.7	7.16				12	13	19	15	16
U									0.87	0.75	0.78	0.93	0.56	0.5	1	1.5								
Ce									30.36	29.27	32.61	26.72	20.27	24.5	28	39.5								
La									10.47	12.67	12.98	11.69	9.75	12.5	13.5	19								
Cs									14.8	11.28	11.15	13.4	3.84	27.6	7.8	3.4								
Sm									3.53	3.3	3.54	3.49	2.46	3	3.5	4								
Nd									23.9	13.92	14.47	13.67	10.08	12.5	14.5	18								
Er									2.38	2.17	2.23	2.57	1.4	2.5	2.6	2.3								
Eu									0.98	0.92	0.9	1.04	0.64	1.2	1	0.8								
Ga									17.07	16.21	15.89	16.69	15.01	22	18	15								
Gd									3.63	3.55	3.58	3.73	2.23	3.6	3.8	3.3								
Hf									2.75	2.35	2.3	2.71	1.74	2	1	3								
Ho									0.91	0.86	0.85	0.98	0.53	0.8	0.9	0.7								
Dy									3.79	3.56	3.49	4.05	2.19	3.9	4.5	3.4								
Lu									0.15	0.34	0.35	0.39	0.22	0.4	0.4	0.4								
Pr									3.68	3.42	3.66	3.34	2.6	3.3	3.5	4.8								
Tb									0.56	0.52	0.53	0.6	0.35	0.6	0.7	0.5								
Tm									0.38	0.35	0.35	0.41	0.22	0.3	0.4	0.4								
Yb									2.31	2.32	2.23	2.51	1.4	2.3	2.3	2.4								
Th/Ta									8	7	7	8		3	3	14								
Nb/Ta									10	11	11	12	6	3	5	12								
La/Nb									1	2	2	2	3	3	2	3								
Th/Ce									0.19	0.15	0.13	0.19	0.14	0.16	0.14	0.18								
Ce/Pb									7.6	4.9	5.4	8.9	0.3	4.9	9.3	9.9								
(La/Yb)cn									4.0	3.7	3.9	3.1	4.7	3.6	3.9	5.3								

Samples with REE provided were analysed using ICP-MS at Chemex (Canada). Other samples were analysedusing XRF at Osaka City University (Japan). LM = Lwabwe plutonic mafic complex; KM = Kidilo orthoamphibolite complex. Mg no. = molar ratio ($Mg/(Mg + Fe^{2+})$), with $Fe^{3+}/Fe^{2+} = 0.2$.

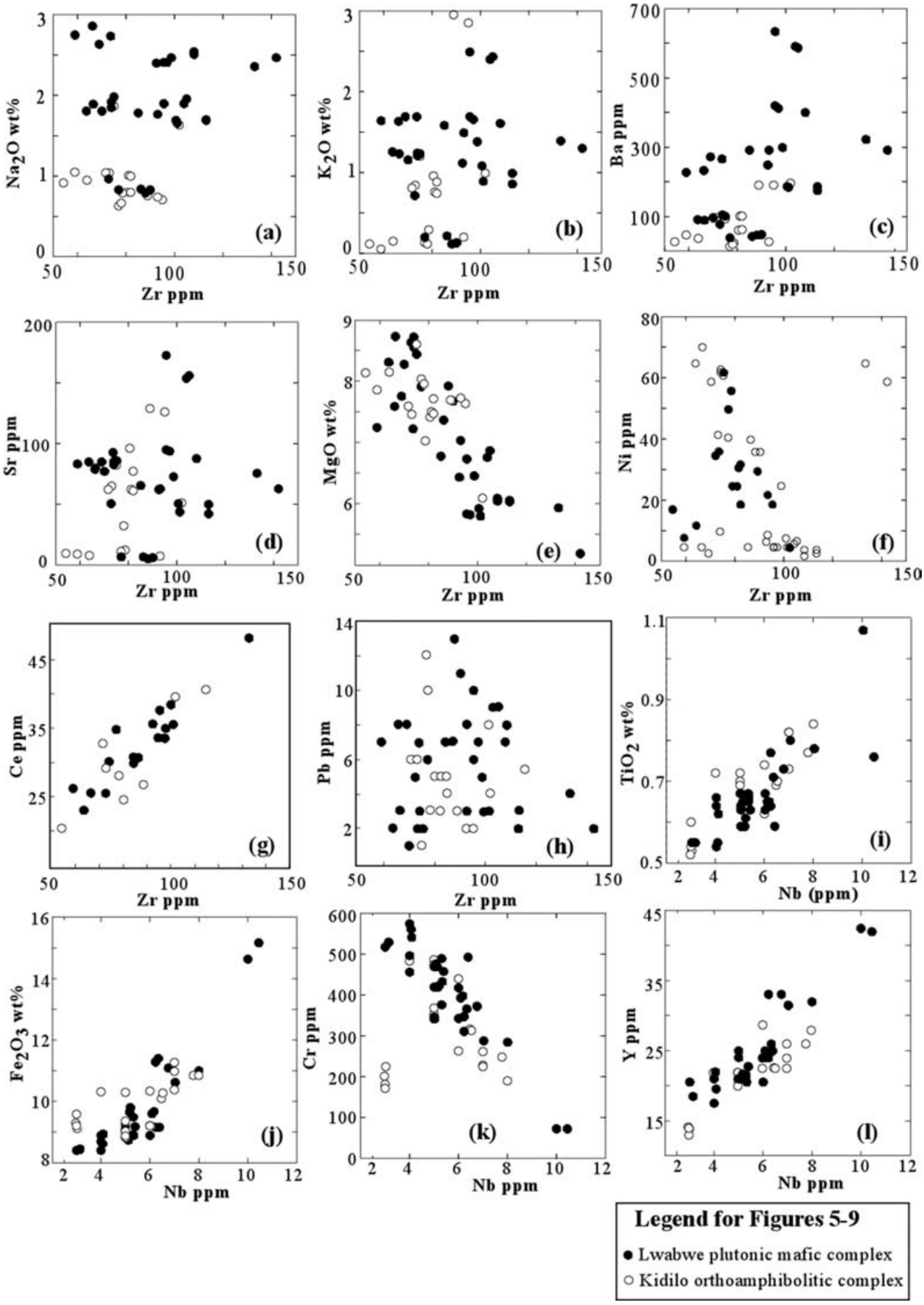

Figure 5. Plots of major and trace elements v. Zr and Nb for Mitwaba mafic–intermediate igneous complexes. See text for details.

https://doi.org/10.1017/S0016756804009951 Published online by Cambridge University Press

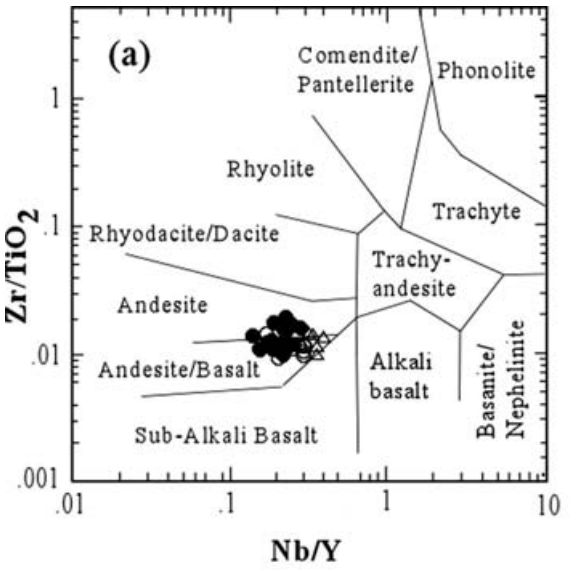

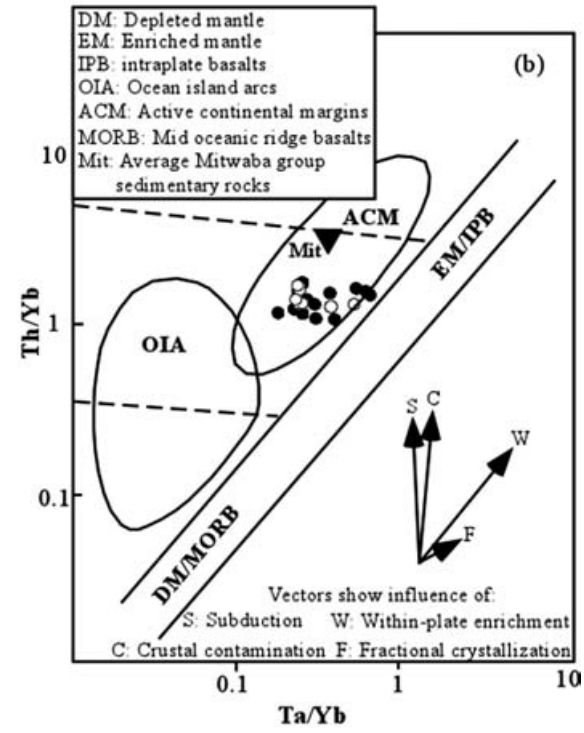

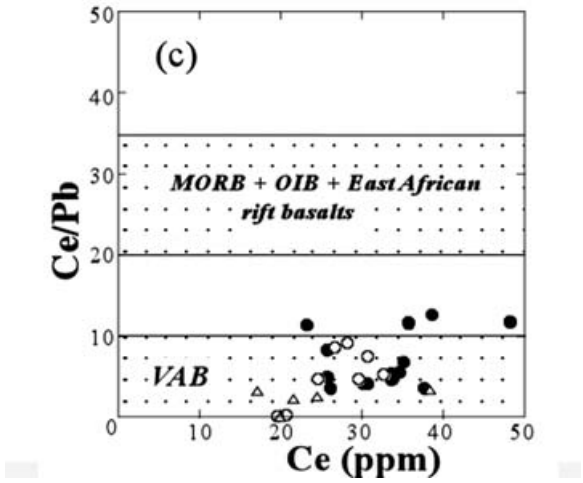

these intrusions consist of metamorphosed diorite and gabbro. Al_2O_3 concentrations are in the range 13–19 wt %. Mg no. is between 40 and 66 (Table 2). All of the samples have low TiO_2 contents (0.52–0.92 %), except in sample LM4, which contains 1.08 % TiO_2. The samples also show low Nb (3–8 ppm), except the same sample LM4, which contains 10 ppm Nb. In contrast, continental tholeiites such as those exposed in the East African rift system are characterized by high TiO_2 values, higher than one (between 1.36 ± 0.12 and 2.02 ± 0.42 %), and also show Nb > 20 ppm, up to 75 ppm (e.g. Kampunzu & Mohr, 1991; Kampunzu *et al*. 1998). MgO decreases with increase in Zr (Fig. 5). Zr ranges from 48 to 142 ppm, Y from 20 to 43 ppm and Ta from < 0.5 to 2 ppm. Ti/Zr ratio is between 31 and 66. This ratio is higher (90–110) in continental tholeiites such as the Deccan basalts (e.g. Dupuy & Dostal, 1984).

Diagrams using the immobile trace elements Ti, Zr and Y have been widely employed for discriminating mafic igneous rocks from various tectonic settings. The discrimination diagrams using these elements (e.g. Figs 6a, 7b) indicate that Mitwaba mafic–intermediate plutonic rocks resemble volcanic-arc rocks. Their Th/Ta and La/Nb ratios range between 3–14 and 2–5, respectively. Nb/Ta values are subchondritic, in the range 8–13 for most mafic rocks with MgO contents higher than 6 %. For comparison, MORB and OIB are, at similar MgO contents, characterized by Nb/Ta of 17 ± 1, similar to the value for the Bulk-Silicate Earth (Kamber & Collerson, 2000 and references therein). Continental crust rocks are characterized by Nb/Ta between 10 and 15. Lower values mark veins deposited by fluids from dehydration under high-pressure metamorphism (blueschist and eclogite facies) of subducting oceanic slabs (Kamber & Collerson, 2000).

In the Th–Ta–Yb discrimination diagram (Pearce, 1983), all mafic rock samples plot in the active continental margin field (Fig. 6b). Ce/Pb in these rocks is in the range 0.3–12 (average ~ 7, N = 25). In the plot of Ce v. Ce/Pb (Fig. 6c), the Mitwaba mafic–intermediate plutonic rocks display similarities with arc rocks. These igneous rocks are also marked by Th/Ce ratios in the range 0.12–0.20, similar to values in mafic arc rocks (e.g. Hawkesworth *et al*. 1997). For comparison, continental tholeiites in the East African

Figure 6. (a) Classification of the Mitwaba mafic–intermediate plutonic rocks using the diagram log (Nb/Y) v. log (Zr/TiO_2). Fields after Winchester & Floyd (1977). (b) Plot of Th/Yb v. Ta/Yb for Mitwaba mafic–intermediate plutonic rocks. (c) Ce/Pb v. Ce diagram showing the fields for OIB-MORB-East African Rift basalts and arc basalts. Also shown in Figure 6a, c (open triangles) are average compositions of Mesoproterozoic mafic igneous rocks from the northern Kibaran belt (data from Evans *et al*. 2000).

https://doi.org/10.1017/S0016756804009951 Published online by Cambridge University Press

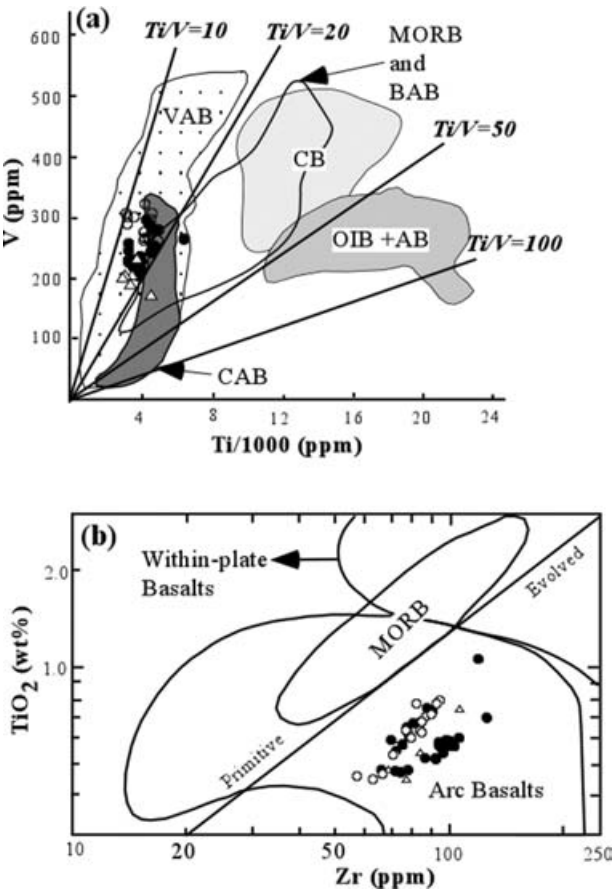

Figure 7. Chemical discrimination diagrams for Mitwaba mafic–intermediate plutonic rocks and comparison with correlative mafic rocks from the northern Kibaran belt in Tanzania. (a) Ti v. V diagram of Shervais (1982). VAB, MORB, CB, CAB, OIB, AB and BAB represent volcanic arc, mid-oceanic ridge, continental, calc-alkaline, oceanic island, alkali basalts and back-arc basalts respectively. (b) Zr–TiO_2 discrimination diagram of Pharaoh & Pearce (1984). See Figures 5 and 6 for explanation of symbols.

rift system (Kampunzu & Mohr, 1991) and those related to the opening of Atlantic in west and northwest Africa (e.g. Bertrand, 1991) are characterized by Th/Ce between 0.06 and 0.10. Mid-ocean ridge basalts (MORB) and ocean island basalts (OIB) are marked by lower Th/Ce ratios between ~ 0.016 and 0.051.

Cr contents decrease with increase in Nb (Fig. 5). The studied rocks have Ni contents between 2 and 70 ppm, which are lower than values for primitive basaltic magmas (300–400 ppm; Sato, 1977). Vanadium contents range between 205 and 320 ppm, and the Ti/V ratios in these rocks define a narrow range between 10 and 19. Sample LM4 has higher TiO_2 contents, yielding a higher Ti/V value close to 24. For comparison, Ti/V ratios in basalts emplaced in extensional tectonic settings far away from any convergent plate boundary (including within-plate basalts) are in the range 20–50 (Shervais, 1982). Continental tholeiites related to the opening of the Atlantic in west and northwest Africa are marked by Ti/V ratios between 23 and 36 (e.g. Bertrand, 1991). In the Ti v. V diagram (Shervais, 1982), Mitwaba mafic–intermediate plutonic rocks plot in the field for arc basalts (Fig. 7a).

Whole-rock geochemical compositions suggest that there are close affinities between samples from the Lwabwe metagabbro and those from Kidilo orthoamphibolites. Both major and trace elements show similar relative abundances and define a single evolution trend in Figure 5, especially for MgO, Cr and Ni, suggesting that the mafic and intermediate igneous rocks in these two complexes are genetically related.

Chondrite-normalized REE patterns (Fig. 8a, b) are marked by light REE (LREE) enrichment and moderate fractionation of heavy REE (HREE), with $(La/Yb)_N$ in the range 2.9–5.8. The REE patterns display a moderate Eu negative anomaly ($Eu/Eu^* = 0.7–0.8$). The multi-element diagram patterns of representative samples of the Mitwaba mafic–intermediate plutonic rocks (Fig. 8c, d) display enrichment in LILE compared to HFSE, with a positive Th anomaly and negative Nb and Ti anomalies. Ta_N (12–36) is lower than La_N but higher than Nb_N, indicating a decoupling between the geochemical behavior of Nb–Ta, consistent with the subchondritic Nb/Ta ratios in these mafic–intermediate rocks. The significance of these observations will be discussed below.

7. Geochronology

7.a. Lwabwe complex (sample LM507)

Zircons extracted from this sample were pink to yellow, prismatic to needle-like and non-translucent (metamict). Back-scattered imaging (Fig. 9a, b) reveals complex internal zoning and the presence of cores in some cases. Eight single zircon grains were analysed and data are reported in Table 3 and plotted in a concordia diagram in Figure 10a. Most zircons are significantly high in common Pb (Table 3); this could be the consequence of their metamict states. The analyses plot in discordant to very discordant positions and do not define a simple, single group or trend (Fig. 10a), which may indicate the presence of more than one age population and probably the effects of more than one Pb-loss event. This scattering of the data is also a consequence of the presence of inherited cores in some of the grains. One grain (1.8, Table 3) is 51 % discordant and gives a $^{207}Pb/^{206}Pb$ date of 1757 ± 3.9 Ma. A regression through all the data except 1.8 gives an upper intercept date of 1278 ± 64 Ma with a very large MSWD of 306. This date is younger than the igneous crystallization age of the Lwabwe metagabbro constrained by field relations (see above) to be older than the Fwifwi foliated leucomonzogranite, emplaced at 1372 ± 9.6 Ma (Kokonyangi *et al*. 2004*a*). Although it appears difficult to calculate an age for this sample, a tentative regression through three zircon analyses (1.1,

https://doi.org/10.1017/S0016756804009951 Published online by Cambridge University Press

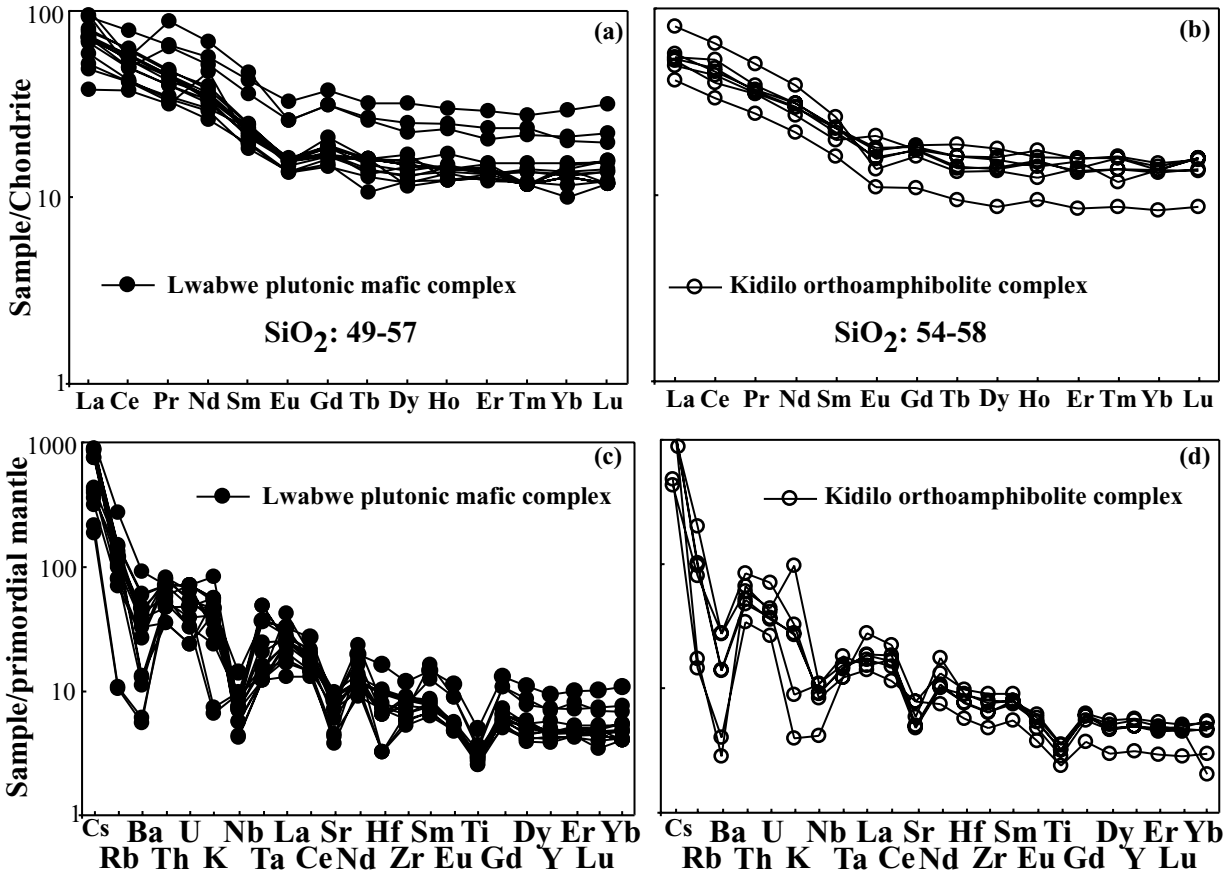

Figure 8. (a, b) Chondrite-normalized REE patterns; (c, d) primordial mantle-normalized spider diagrams for Mitwaba mafic–intermediate plutonic rocks. Normalizing values after Sun & McDonough (1989). Legend as in Figure 5.

1.2, 1.3) yields a well-defined upper intercept date of 1376 ± 13 Ma (MSWD = 0.046) and a lower intercept date of 520 ± 14 Ma.

7.b. Kidilo orthoamphibolite complex (sample KM407)

Zircons from this complex are pink, rounded to sub-rounded, metamict (Fig. 9b, c), and present fairly high common Pb contents (Table 3). The rounded to sub-rounded shape of the zircon grains from this sample could result from resorption during amphibolite-facies metamorphism. Back-scattered imaging reveals the presence of cores and rims. Most of the eight analyses performed on zircons from this sample (Table 3) are highly discordant and are scattered in the concordia diagram (Fig. 10b). As for sample LM507, it is therefore difficult to calculate an age for this sample. The oldest xenocrystic date is provided by analysis 2.2, with a $^{207}Pb/^{206}Pb$ date of 1836 ± 2.3 Ma. A single zircon analysis (2.4) lies very close to concordia (97 % concordant). It yields a $^{207}Pb/^{206}Pb$ date of 1417 ± 1.7 Ma. The same analysis yields $^{207}Pb/^{235}U$ date of 1390 ± 1.7 Ma, while two grains (2.3 and 2.5) plot very close to concordia and have a mean $^{206}Pb/^{238}U$ date of 560 Ma.

The uranium contents discriminate zircons from Mitwaba 1.38 Ga granitoids (Kokonyangi *et al*. 2004*a*) and those from geographically related mafic–intermediate igneous rocks described in this paper (Fig. 11). Zircons from the felsic rocks are characterized by U < 600 ppm, whereas those from the mafic rocks have U > 600, up to 2500 ppm (except for zircon 2.4, sample KM 470, containing 450 ppm, Table 3). Figure 11 shows that zircons from mafic and felsic rocks are different in terms of U contents. These contrasting zircon chemical features reflect distinct igneous zircon populations.

8. Discussion

This discussion will focus on assessing the timing of emplacement of the Mitwaba mafic–intermediate plutonic igneous rocks and on their tectonic setting. There are currently two main models proposed to explain the genesis of early Kibaran (1.4–1.35 Ga) mafic and felsic igneous rocks in the Kibaran belt. The first model was proposed by Kampunzu *et al*. (1986) and expanded by Kokonyangi *et al*. (2004*a*). It assumes that the early Kibaran igneous rocks were emplaced during plate convergence, most probably along an active continental margin resulting from

https://doi.org/10.1017/S0016756804009951 Published online by Cambridge University Press

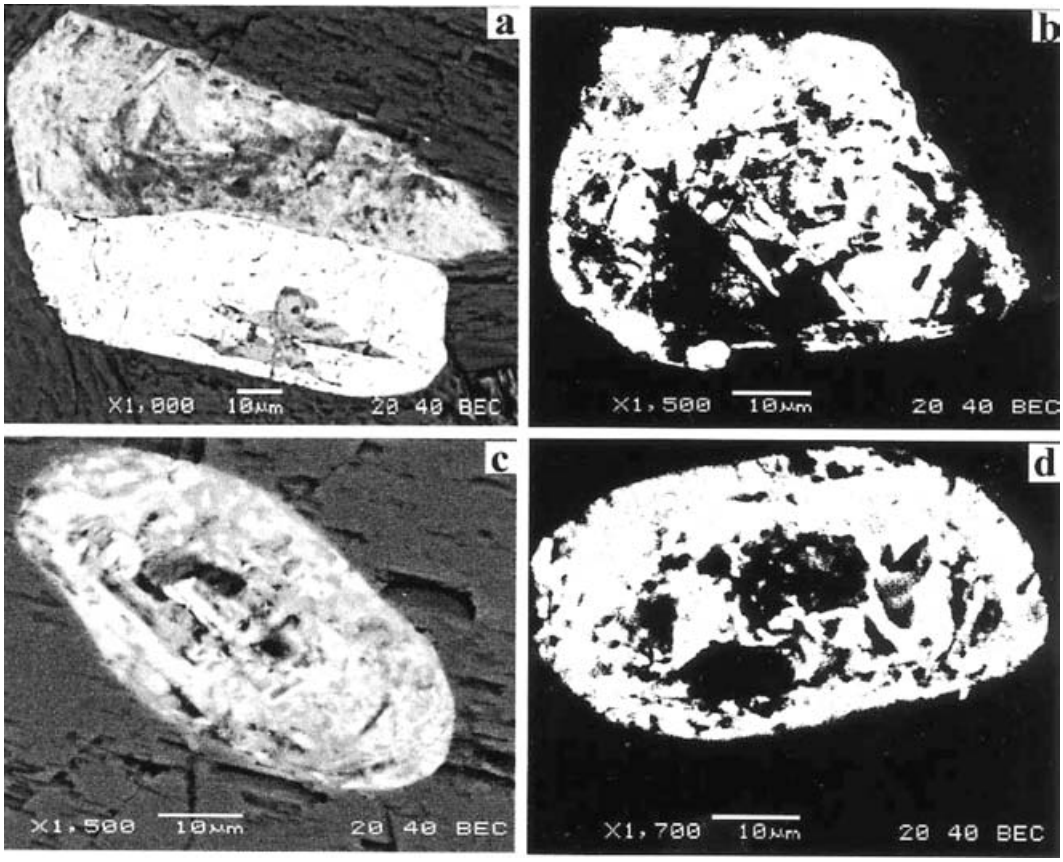

Figure 9. Back-scattered electron images of zircons from Mitwaba mafic–intermediate plutonic rocks. (a) Prismatic, primary oscillatory zoned zircon grain (light grey) in sharp contact with igneous magnetite crystal (bright). Sample from Lwabwe plutonic mafic complex. Note that both grains are included within a prismatic primary hornblende. (b) A fragment of zircon grain showing a metamict core rimmed by prismatic magmatic zircon. Sample from Lwabwe plutonic mafic complex. (c) Oscillatory zoned zircon containing unzoned, inherited core. (d) Centre of unzoned, metamict zircon surrounded by a thick band of weakly zoned to unzoned zircon. BSE images were taken on thin sections cut from samples LM507 and KM407.

convergence between the Congo craton to the northwest and the Tanzania–Bangweulu craton to the southeast. The second model, proposed by Klerkx *et al*. (1987) and expanded by Fernandez-Alonso & Theunissen (1998), links the early Kibaran magmatism to a bimodal igneous suite emplaced in an extensional rift setting. Geochronological and geochemical data presented in this paper provide critical constraints for these models.

8.a. Age of the early Kibaran magmatism

Field observations indicate that the Mitwaba plutonic mafic complexes exhibit chilled margins against the Mitwaba group metasedimentary rocks and are disconformably overlain by the Mulumbi group units. Both mafic complexes are thermally affected by the emplacement of the Kifinga–Kisele batholith, leading to the growth of garnet, biotite and ferro-tschermakite. Furthermore, the granitoids contain angular xenoliths of Lwabwe and Kidilo mafic igneous complexes. These observations indicate that the mafic igneous complexes pre-date the emplacement of the 1.38 Ga granitoids, but available U–Pb geochronology is consistent with the emplacement of all the igneous rocks within a short time interval.

The upper intercept date of 1376 ± 13 Ma for sample LM507 represents the best estimate for the igneous crystallization age of the Lwabwe plutonic mafic rocks. One zircon grain from the Kidilo orthoamphibolite (sample KM 407) yields a 97 % concordant analysis, with a $^{207}Pb/^{206}Pb$ date of 1417 ± 1.7 Ma, which represents the best estimate of the minimum age of crystallization of the Kidilo amphibolite. Another interpretation of this date would be that the analysis 2.4 contains a minor inherited component. If indeed there is any inheritance, this inheritance will as well affect the $^{207}Pb/^{235}U$ and the $^{206}Pb/^{238}U$ ages and therefore one cannot use either of these two ages as they are systematically younger than the 'real' igneous ages for these orthoamphibolites. The best way in this case is to consider the $^{207}Pb/^{206}Pb$ age as the minimum age of crystallization of these rocks. It is indeed possible that this grain had some inheritance, but available data do not allow confirmation of this at the moment. Although it is difficult to define precisely the igneous crystallization age for the Kidilo

https://doi.org/10.1017/S0016756804009951 Published online by Cambridge University Press

Table 3. U–Pb zircon isotopic data

	U (ppm)	Th/U	$^{206}Pb/^{204}Pb$	Pbc (pg)	Pb* (ppm)	$^{206}Pb/^{238}U$	Error (%)	$^{207}Pb/^{235}U$	Error (%)	$^{207}Pb/^{206}Pb$	Error (%)	$^{206}Pb/^{238}U$ (Ma)	$^{207}Pb/^{235}U$ (Ma)	$^{207}Pb/^{206}Pb$ (Ma)	±	Disc. (%)
Sample LM507																
1.1	729	0.509	200	181	146	0.17811	0.204	2.01091	0.316	0.081885	0.206	1057	1119	1243	4.0	16.2
1.2	2445	0.723	627	188	450	0.14809	0.173	1.58822	0.206	0.077784	0.079	890	966	1141	1.6	23.6
1.3	1807	0.616	123	442	349	0.16299	0.173	1.80145	0.356	0.080163	0.262	973	1046	1201	5.2	20.4
1.4	1282	0.703	3571	19	264	0.17325	0.2	1.89348	0.211	0.079265	0.059	1030	1079	1179	1.2	13.6
1.5	2148	1.018	241	540	492	0.17694	0.167	1.96512	0.250	0.080550	0.148	1050	1104	1210	2.9	14.3
1.6	1491	1.228	426	79	202	0.11601	0.165	1.15986	0.221	0.072510	0.118	708	782	1000	2.4	30.9
1.7	1564	0.319	120	406	282	0.10576	0.228	1.07110	0.437	0.073451	0.324	648	739	1026	6.6	38.8
1.8	319	0.310	320	10	52	0.15229	0.298	2.25688	0.299	0.107485	0.213	914	1199	1757	3.9	51.4
Sample KM407																
2.1	695	0.323	4899	3	150	0.21244	0.195	2.52385	0.193	0.086166	0.084	1242	1279	1342	1.6	8.2
2.2	297	0.299	718	10	64	0.19752	0.302	3.05677	0.3	0.112238	0.126	1162	1422	1836	2.3	40.05
2.3	251	0.233	124	22	24	0.09101	0.280	0.79001	1.095	0.062959	0.995	562	591	707	21.2	21.5
2.4	916	0.180	3047	9	214	0.23720	0.237	2.92978	0.238	0.089582	0.090	1372	1390	1417	1.7	3.5
2.5	373	0.193	240	10	35	0.09054	0.827	0.74820	1.332	0.059937	0.986	559	567	601	21.3	7.4
2.6	1260	0.155	866	29	193	0.15401	0.251	1.74283	0.268	0.082072	0.123	923	1025	1247	2.4	27.9
2.7	865	0.345	776	40	173	0.18856	0.186	2.50315	0.207	0.096279	0.094	1114	1273	1553	1.9	30.8
2.8	450	0.308	1659	3	100	0.21484	0.255	2.65905	0.258	0.089765	0.091	1255	1317	1421	1.7	12.9

Errors are listed at 2σ; Pbc and Pb* indicate common and radiogenic lead, respectively.
Samples LM507 and KM407 are from the Lwanbwe plutonic mafic and Kidilo orthoamphibolite, respectively.

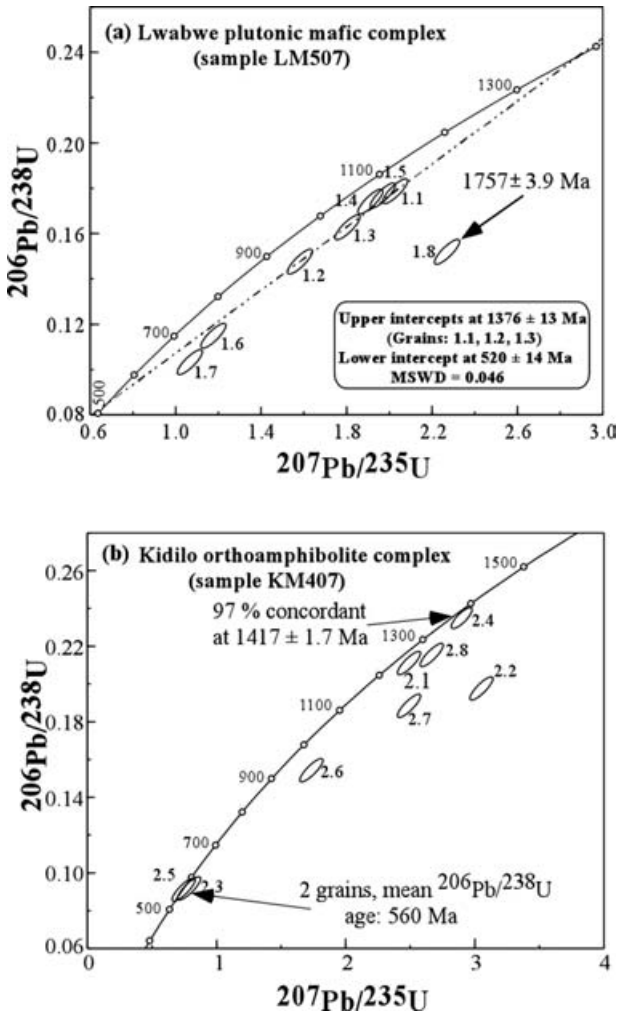

Figure 10. U–Pb concordia diagrams of zircons from Mitwaba mafic–intermediate plutonic rocks. (a) Lwabwe complex (greenschist facies; sample LW507). (b) Kidilo complex (amphibolite facies; sample KM 407). For both diagrams, the data-point error ellipses are plotted with two sigma errors. See text for more details.

orthoamphibolite, the data in Table 3 and Figure 10b are consistent with emplacement of both Lwabwe and Kidilo complexes in a similar time frame, at *c*. 1.39–1.38 Ga. Strongly peraluminous syn-D_1 Kibaran granitoids geographically associated with the Mitwaba mafic–intermediate plutonic rocks yielded SHRIMP U/Pb zircon concordant crystallization ages of 1381 ± 8 Ga in the Mitwaba area (Kokonyangi *et al*. 2001, 2004*a*) and ~ 1370 Ma (errors not given) in the western internal zone of the northern Kibaran belt in Burundi (Tack *et al*. 2002). These data indicate that a large amount of strongly peraluminous granitoids and spatially associated mafic–intermediate plutonic rocks exposed over the *c*. 3000 km long Kibaran belt in eastern central Africa were emplaced over a short period of time. An alternative interpretation of the above data would be that the Mitwaba mafic–intermediate plutonic rocks post-date the granitoids and incorporated xenocrystic zircons from the adjacent 1.38 Ga

https://doi.org/10.1017/S0016756804009951 Published online by Cambridge University Press

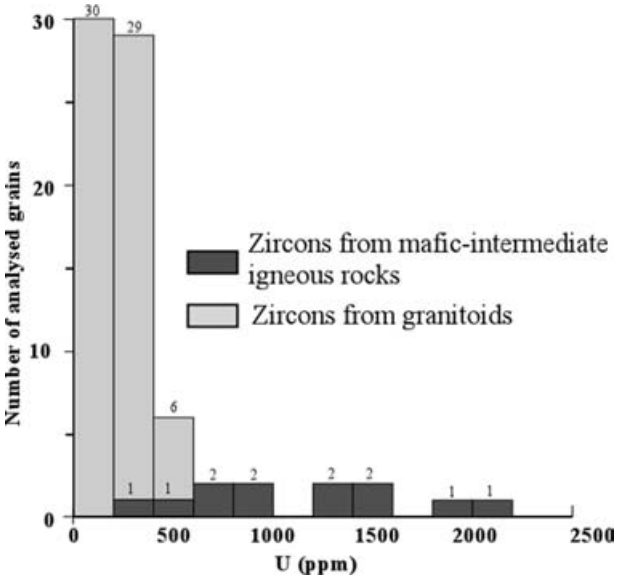

Figure 11. Histogram showing distinct uranium concentrations for zircons from 1.38 Ga Mitwaba granitoids and mafic–intermediate plutonic rocks. Xenocrystic zircons and discordant zircons yielding Palaeoproterozoic and Neoproterozoic apparent dates, respectively, are excluded.

Kifinga–Kisele granitic batholith en route to the surface. However, this possibility is ruled out by field data indicating that the granitoids intrude the mafic plutonic bodies. In addition, as shown in Figure 11, zircons from mafic and felsic rocks are different in terms of U contents. Consequently, the protoliths of the Mitwaba mafic igneous rocks and felsic orthogneisses could be broadly coeval at 1.38 Ga. Thus, tectonic models for the Kibaran orogenic system at ~1400–1350 Ma must accommodate the generation of large volumes of magmas, including mafic arc igneous rocks and strongly peraluminous felsic melts, during the early stages of the orogeny. Any valid model must account for the fact that the Mitwaba mafic–intermediate plutonic rocks and geographically associated strongly peraluminous granitoids are broadly coeval and pre-date the continental collision event dated at *c*. 1079 ± 14 Ma in the Mitwaba area (Kokonyangi *et al*. 2001, 2004*a*). At the scale of the Kibaran belt, Kampunzu *et al*. (1998 and unpub. data) indicated that igneous rocks with crystallization ages < 1.25 Ga display geochemical features linking them to continental collision and related late- to post-orogenic extensional collapse. The lower intercept date of *c*. 520 ± 14 Ma shown by analyses 1.1, 1.2 and 1.3 from the sample LM507 and the date of *c*. 560 Ma from sample KM407 (Fig. 10) could possibly mark Pan-African reworking of the Kibaran terrains (and their zircons) in the Mitwaba area, particularly because Neoproterozoic Katangan sedimentary rocks are exposed < 10 km south of the study area (e.g. Fig. 1a, b). However, this possibility is ruled out because the Neoproterozoic rocks exposed near Mitwaba are undeformed and unmetamorphosed. Furthermore, it is known that lower intercept ages may be significant only if they are defined by zircons with U < 100 ppm (Mezger & Krogstad, 1997), and this is not the case for zircons from the Mitwaba mafic–intermediate plutonic rocks.

8.b. Rift setting

Huppert & Sparks (1988) and Annen & Sparks (2002) stressed the important role of mafic magmas in the generation of granitic melts in the crust. Similarly, experimental work (e.g. Patiño-Douce, 1995) showed that a large amount (up to 40 %) of felsic melts (> 70 % SiO_2) could be generated by interaction of mafic magma with metapelitic material of the type present in large amounts in the Kibaran belt. This mechanism is important both in volcanic arc (e.g. Hyndman & Foster, 1989) and extensional settings (e.g. Bergantz, 1989; Fountain, 1989). In continental rift settings, the emplacement of such large volumes of felsic melts requires a huge amount of mafic magma derived from uprising asthenosphere. Klerkx *et al*. (1987) and Fernandez-Alonso & Theunissen (1998) interpreted early Kibaran felsic and mafic igneous rocks in terms of rift-related magmatism. Their interpretation assumes also that the Congo and the Tanzania–Bangweulu cratons existed as a single cratonic block before the Kibaran orogeny. The lack of a possibility of geological and geochronological correlations between rock units of the Congo (W) and Tanzania–Bangweulu (E) cratons (present day coordinates) on both sides of the Kibaran belt indicates that these two cratons were unrelated before their late Mesoproterozoic assembly. The interpretation of Klerkx *et al*. (1987) and Fernandez-Alonso & Theunissen (1998) is also not supported by: (1) geochemical data of Ntungincimpaye & Kampunzu (1987) requiring a mantle source enriched during subduction for mafic igneous rocks exposed in the internal zone of the Kibaran belt in Burundi; and (2) structural data, which indicate that early Kibaran granitoids were emplaced during the compressional D_1 Kibaran deformation event marked by asymmetric folds and reverse faults/thrusts (Kampunzu *et al*. 1986; Rumvegeri, 1991; Kokonyangi *et al*. 2004*a*, *b*).

The geochemical compositions of mantle-derived mafic rocks emplaced in pristine continental rifts such as the East African Rift record a substantial input from the asthenospheric reservoir, suggesting plume uprise as the driving force behind the rifting process. Mafic igneous rocks related to plume activity in continental rift systems away from plate convergent margins are marked by La/Nb < 1.5 and Ce/Pb ~ 25 (Kampunzu & Mohr, 1991; Kampunzu *et al*. 1998), and the same values mark asthenospheric melts in other continental and oceanic extensional settings (Fitton *et al*. 1988; Saunders *et al*. 1992; Chauvel, Goldstein, & Hofmann, 1995). The low La/Nb and high Ce/Pb ratios in the East African Rift System basalts are similar to those reported in OIB and MORB (e.g. Fig. 6c). La/Nb ratios

https://doi.org/10.1017/S0016756804009951 Published online by Cambridge University Press

higher than 2 (up to 5) and patterns on chondrite-normalized REE and primordial mantle-normalized spider diagrams (Fig. 8a–d) do not support involvement of asthenospheric mantle as the source of the Mitwaba mafic plutonic rocks. The elemental contents, inter-element ratios and mantle-normalized patterns contrast with those marking continental tholeiites unrelated to plate convergence process (e.g. Kampunzu & Mohr, 1991; Bertrand, 1991). The geochemical data, in conjunction with structural data and the regional setting, preclude an intracontinental rift environment during the emplacement of the 1.38 Ga mafic–intermediate plutonic rocks.

8.c. Active continental margin

Structural investigations indicate that the Kibaran belt was undergoing compression during the emplacement of the mafic–intermediate plutonic rocks and coeval, strongly peraluminous granitoids (Kampunzu *et al*. 1986; Rumvegeri, 1991; Kokonyangi *et al*. 2002, 2004*a*). Mitwaba mafic–intermediate plutonic rocks show distinctive patterns in multi-element diagrams marked by a progressive decrease from left to right across the diagram, accompanied by Nb and Ti negative anomalies (Fig. 8c, d). These features are usually observed in mafic igneous rocks from convergent plate margins (Pearce, 1982, 1983) and in continental tholeiites originating from partial melting of a lithospheric mantle enriched during a subduction event.

High Th/Ta ratios mark the studied rocks, which also display low TiO_2 and Nb contents. These features are common in mafic arc rocks, although they are also known in some basalts derived from old subduction-enriched lithospheric mantle (e.g. Ormerod *et al*. 1988). In contrast, basalts originating from an asthenospheric reservoir show generally low Th/Ta (< 2) and La/Nb (< 1.5), with high TiO_2 and Nb contents. Continental tholeiites such as those related to the East African rift system and to the opening of Atlantic (e.g. Kampunzu & Mohr, 1991; Bertrand, 1991) are also marked by low Th/Ta (< 2) ratios and relatively high TiO_2 (> 1 up to 3 wt %). Data in this paper indicate that none of the studied mafic rocks, including the least deformed and metamorphosed ones, display chemical characteristics of asthenospheric mafic melts. The high Th/Ta ratios, low Nb/Ta ratios and relatively low HFSE (Ti, Nb, Ta; Table 2) abundances suggest a subduction process during which the mantle wedge was enriched in LILE and impoverished in HFSE from dehydration of a down-going slab, possibly with additional input of partial melts from subducted sediments (e.g. Plank & Langmuir, 1993, 1998; Pearce & Peate, 1995; Kamber & Collerson, 2000). Two important features observed in the Mitwaba mafic–intermediate plutonic rocks are the low ratios of fluid-immobile over fluid-mobile elements, such as Ce/Pb (Fig. 6c) and the decoupling of Nb/Ta, leading to subchondritic ratios lower than 10 in mafic rocks with MgO contents > 6 %; these two geochemical signatures likely reflect a substantial input of fluids from the dehydration of a subducting slab (e.g. Hawkesworth *et al*. 1997). The mantle wedge above relatively steep subducting slabs is usually enriched by hydrous fluids originating from the breakdown of hydrous phases (e.g. Luhr, 1992). This process results in the fractionation of the couple Nb–Ta and the depletion of the mantle wedge in HFSE with respect to LILE (cf. high La/Nb ratios in arc magmas) and enrichment in mobile elements (K, U, Ba and Sr). Pb is also enriched compared to Ce, resulting in low Ce/Pb ratios common in arc mafic magmas. Hawkesworth *et al*. (1997) indicated that Th, LREE and Ta are not mobilized in the fluids from the dehydration of the subducting slab and suggested that their contents in most arc-related mafic rocks should be attributed to the input of partial melt from sediments entrained by the down-going oceanic crust. However, in the case of Ta, Kamber & Collerson (2000) showed that locally derived metamorphic veins hosted in blueschist- and eclogite-facies mafic rocks and interpreted to represent the composition of fluids from dehydration of subducting oceanic slabs yield very low Nb/Ta ratios between 2 and 5, lower than values recorded in sedimentary rocks. In addition, Hawkesworth *et al*. (1997) showed that mafic arc rocks originating from a mantle source enriched by subducted sediments are marked by Th/Ce ratios close to 0.20. Th/Ce and Nb/Ta ratios in mantle derived melts formed far away from plate convergent systems, including MORB and OIB, are between ~ 0.016–0.051 and $\sim 17 \pm 1$, respectively (e.g. Sun & McDonough, 1989). Continental tholeiites marking extensional systems far from any plate convergence (e.g. Kampunzu & Mohr, 1991; Bertrand, 1991) are also marked by Th/Ce ratios ≤ 0.10. In contrast, the Mitwaba mafic–intermediate plutonic rocks have Th/Ce ratios between 0.12 and 0.19 (average 0.16, 24 samples, Table 2), similar to values recorded in arc mafic magmas. Therefore, we infer that the high Th/Ce and Th/Ta ratios coupled to low Ce/Pb and Nb/Ta ratios in the Mitwaba mafic–intermediate plutonic rocks are primarily due to subduction processes, that is, mantle-wedge enrichment by fluids and contribution from subducted sediments. Isotopic investigations are required in order to constrain this interpretation.

A model involving underplating of mafic–intermediate arc magma in the crust, causing partial melting of Mitwaba group metasedimentary rocks during the accretionary stage of the Kibaran orogeny, is suggested to explain the association of 1.38 Ga mafic–intermediate arc rocks and strongly peraluminous granitoids exposed over the *c*. 3000 km long Kibaran belt of central Africa. Similar magmatic associations are known in the Lachlan fold belt of Australia and Hercynian belt of Europe (e.g. Bea, Montero & Molina, 1999), suggesting that these belts could have experienced the same geological history as the Kibaran belt of central Africa.

https://doi.org/10.1017/S0016756804009951 Published online by Cambridge University Press

9. Conclusions

(1) U–Pb single zircon geochronology shows that Mitwaba mafic–intermediate plutonic rocks were emplaced at 1376 ± 13 Ma (Lwabwe plutonic mafic complex), although a sub-concordant zircon yields a $^{207}Pb/^{206}Pb$ date of 1417 ± 1.7 Ma (Kidilo orthoamphibolite complex), indicating that the earliest phase of these mafic–intermediate plutonic rocks could be slightly older. These mafic–intermediate plutonic rocks are coeval with the strongly peraluminous 1.38 Ga granitoids exposed in the Mitwaba area (southeastern Congo). Mitwaba mafic–intermediate plutonic rocks are coeval with mafic rocks documented in the Burundian segment of the Kibaran belt, and both groups of rocks are part of the early Kibaran felsic and mafic magmatism, pointing to a major syn-kinematic D_1 igneous event in the Kibaran belt at ∼ 1.38 Ga.

(2) Although subsolidus metamorphic recrystallization led to partial replacement of igneous minerals and textures by greenschist–amphibolite-facies parageneses, the whole-rock chemical composition of variably metamorphosed Mitwaba mafic–intermediate plutonic rocks, with and without primary textures preserved, and the geochemical plots involving immobile elements (e.g. HFSE, REE) indicate that the studied mafic–intermediate plutonic rocks contrast with within-plate basalts, continental rift-related mafic igneous rocks and MORB. The data in this paper suggest that the Mitwaba mafic–intermediate plutonic rocks originated from a mantle wedge enriched during subduction of oceanic crust.

(3) The 1.38 Ga magmatism was emplaced during the D_1 compressional deformation event in the Kibaran belt of central Africa and it is taken to mark the accretionary stage of the belt as suggested by the active continental margin geochemical signature of the Mitwaba mafic–intermediate plutonic rocks. This igneous event was marked by a wide underplating of mafic–intermediate arc magmas within the Mesoproterozoic Kibaran basin, inducing copious partial melting of Kibaran sedimentary rocks to generate the widespread strongly peraluminous granitoids similar to those exposed in the Lachlan and Hercynian fold belts.

Acknowledgements. We acknowledge the constructive reviews of R. Hanson, J.J.W. Rogers and the editor David Pyle that helped to clarify several points in this manuscript. JK acknowledges the financial support from the Japanese Ministry of Education, Science and Culture (MEXT). K. Furuyama (OCU) provided the XRF analyses. S. Yoshikura and Y. Yoshimura (Kochi University) are acknowledged for EPMA chemical mapping of garnet. K. Satish (Shizuoka University) read the early version of the manuscript and J-P. Bulambo (University of Lubumbashi) is thanked for constructive discussions in the field. This is a contribution to the Japanese Society for Promotion of Science (JSPS) Grant-In-Aid for Scientific Research (Project no. 1337005, Leader M. Arima), the IGCP 440 and the Gondwana Institute for Geology and Environment.

References

ANNEN, C. & SPARKS, R. S. J. 2002. Effect of repetitive emplacement of basaltic intrusions on thermal evolution and melts generation in the crust. *Earth and Planetary Science Letters* **203**, 937–55.

ARNDT, N. T. 1983. Element mobility during komatiite alteration. *Eos* **64**, 331.

ARNDT, N. T. 1994. Archaean komatiites. In *Archaean Crustal Evolution*. (eds K. C. Condie), pp. 11–44. Elsevier, Amsterdam.

BARKER, A. J. 1998. *Introduction to metamorphic textures and microstructures*. Stanley Thornes, pp. 1–264.

BEA, F., MONTERO, P. & MOLINA, J. F. 1999. Mafic precursors, peraluminous granitoids, and late lamprophyres in the Avila batholith: a model for the generation of Variscan batholiths in Iberia. *Journal of Geology* **107**, 399–419.

BERGANTZ, G. W. 1989. Underplating and partial melting: implication for the melt generation and extraction. *Science* **245**, 1093–5.

BERTRAND, H. 1991. The Mesozoic tholeiitic province of northwest Africa: a volcano-tectonic record of early opening of central Atlantic. In *Magmatism in extensional structural settings. The Phanerozoic African plate* (eds A. B. Kampunzu and R. T. Lubala), pp. 147–88. Heidelberg: Springer-Verlag.

CAHEN, L. 1954. *Géologie du Congo Belge*. Liège, Belgium, Vaillant-Carmanne, 580 pp.

CAHEN, L., DELHAL, J. & DEUTSCH, S. 1967. Rubidium-strontium geochronology of some granitic rocks from the Kibaran belt (central Katanga, Rep. Congo). *Annale du Musée Royal d'Afrique Centrale in 8°, Science Geologique*, 59 pp.

CAHEN, L., DELHAL, J., VAIL, J. R., BONHOMME, M. & LEDENT, D. 1984. *The geochronology and evolution of equatorial Africa*. Oxford: Clarendon Press, pp. 1–496.

CHAUVEL, C., GOLDSTEIN, S. L. & HOFMANN, A. W. 1995. Hydration and dehydration of oceanic crust controls Pb evolution in the mantle. *Chemical Geology* **126**, 65–75.

DEBLOND, A., PUNZALAN, L. E., BOVEN, A. & TACK, L. 2001. The Malagarazi Supergoup of southeast Burundi and its correlative Bukoba Supergoup of northwest Tanzania: Neo- and Mesoproterozoic chronostratigraphy constraints from Ar–Ar ages on mafic rocks. *Journal of African Earth Sciences* **32**, 435–49.

DUPUY, C. & DOSTAL, J. 1984. Trace elements geochemistry of some continental tholeiites. *Earth and Planetary Science Letters* **67**, 61–9.

EVANS, D. M., BOADI, I., BYEMELWA, L., GILLIGAN, J., KABETE, J. & MARCET, P. 2000. Kabanga magmatic nickel sulphide deposits, Tanzania: Morphology and geochemistry of associated intrusions. *Journal of African Earth Sciences* **30**, 651–74.

FERNANDEZ-ALONSO, M. & THEUNISSEN, K. 1998. Airbone geophysics and geochemistry provide new insights in the intracontinental evolution of the Mesoproterozoic Kibaran belt (central Africa). *Geological Magazine* **135**, 203–16.

FITTON, J. G., JAMES, D., KEMPTON, D. P., ORMEROD, D. S. & LEEMAN, W. P. 1988. The role of lithospheric mantle in the generation of late Cenozoic basic magmas in the western United States. *Journal of Petrology* (Special Lithosphere Issue), 331–49.

FOUNTAIN, D. M. 1989. Growth and modification of lower continental crust in extended terrains: the role of

https://doi.org/10.1017/S0016756804009951 Published online by Cambridge University Press

extension and magmatic underplating. In *Properties and processes in the earth's lower crust* (eds R. F. Mereu, S. Mueller and M. F. Fountain), pp. 287–99. American Geophysical Union Monograph Series no. 51.

HAWKESWORTH, J. C., TURNER, S., PEATE, D. W, MCDERMOTT, F. & VAN CALSTEREN, P. 1997. Elemental Th and U variation in island arc rocks: implications for U-series isotopes. *Chemical Geology* **139**, 207–21.

HUPPERT, H. E. & SPARKS, R. S. J. 1988. The generation of granitic magma by intrusion of basalts into the continental crust. *Journal of Petrology* **29**, 599–624.

HYNDMAN, D. W. & FOSTER, D. A. 1988. The role of tonalites and mafic dykes in the generation of Idaho batholith. *Journal of Petrology* **25**, 894–929.

IKINGURA, J. R., REYNOLDS, P. H., WATKISON, D. H. & BELL, K. 1992. $^{40}Ar/^{39}Ar$ dating of micas from granites of NE Kibaran belt (Karagwe-Ankolean), NW Tanzania. *Journal of African Earth Sciences* **15**, 501–11.

KAMBER, B. S. & COLLERSON, K. D. 2000. Role of "hidden" deeply subducted slabs in mantle depletion. *Chemical Geology* **166**, 241–54.

KAMPUNZU, A. B., AKANYANG, P., MAPEO, R. B. M., MODIE, B. N. & WENDORF, M. 1998. Geochemistry and tectonic significance of Mesoproterozoic Kgwebe metavolcanic rocks in northwest Botswana: implications for the evolution of the Kibaran Namaqua-Natal Belt. *Geological Magazine* **133**, 669–83.

KAMPUNZU, A. B. & MOHR, P. 1991. Magmatic evolution and petrogenesis in the East African Rift System. In *Magmatism in extensional structural settings. The Phanerozoic African plate* (eds A. B. Kampunzu and R. T. Lubala), pp. 65–136. Heidelberg: Springer-Verlag.

KAMPUNZU, A. B., RUMVEGERI, B. T., KAPENDA, D., LUBALA, R. T. & CARON, J. P. 1986. Les Kibaride d'Afrique centrale et orientale: une chane de collision. *UNESCO, Geology for Economic Development, Newsletter* **5**, 125–37.

KLERKX, J., LIEGEOIS, J. P., LAVREAU, J. & CLAESSEN, W. 1987. Crustal evolution of northern Kibaran belt in eastern and central Africa. In *Proterozoic Lithospheric Evolution* (ed. A. Kröner), pp. 217–33. American Geophysical Union, Geodynamic Series no. 17.

KOKONYANGI, J., ARMSTRONG, R., KAMPUNZU, A. B., YOSHIDA, M. & OKUDAIRA T. 2004*a*. U-Pb zircon geochronology and petrology of granitoids from Mitwaba (Katanga, Congo): implications for the evolution of the Mesoproterozoic Kibaran belt. *Precambrian Research* **132**, 79–106.

KOKONYANGI, J., ARMSTRONG, R., KAMPUNZU, A. B., YOSHIDA, M. & OKUDAIRA, T. 2002. Magmatic evolution of the Kibaride belt (Katanga, Congo) and implications for Rodinia reconstruction: Field observations, U–Pb SHRIMP geochronology and geochemistry of granites. In *11th IAGOD Quadrennial Symposium and Geocongress* (ed. Geological Survey of Namibia), p. 5. Geological Survey of Namibia, Windhoek, Namibia.

KOKONYANGI, J., KAMPUNZU, A. B., ARMSTRONG, R., NGULUBE, D. A., YOSHIDA, M. & OKUDAIRA, T. 2004*b*. The Mesoproterozoic Kibarides belt (Katanga, SE Congo). *Journal of African Earth Sciences*, Special Issue, in press.

KOKONYANGI, J., OKUDAIRA, T., KAMPUNZU, A. B. & YOSHIDA, M. 2001. Geological evolution of the Kibaride belt, Mitwaba, Democratic Republic of Congo, Central Africa. *Gondwana Research* **4**, 663–4.

KROGH, T. E. 1973. A low contamination method for the hydrothermal decomposition of zircon and extraction of U and Pb for isotopic age determinations. *Geochimica et Cosmochimica Acta* **37**, 485–94.

KROGH, T. E. 1982. Improved accuracy of U–Pb ages by the creation of more concordant systems using an air abrasion technique. *Geochimica et Cosmochimica Acta* **46**, 617–49.

LEAKE, B. E., WOOLEY, A. R., ARPS, C. E. S., BIRCH, W. D., GILBERT, M. C., GRICE, J. D., HAWTHORNE, F. C., KATO, A., KISCH, H. J., KRIVOVICHEV, V. G., LINTHOUT, K., LAIRD, J., MANDARINO, J. A., MARESH, W. V., NICKEL, E. H., ROCK, N. M. S., SCHUMACHER, J. C., SMITH, D. C., STEPHENSON, N. C. N., UNGARETI, L., WHITTAKER, E. J. W. & YOUZHI, G. 1997. Nomenclature of amphiboles: report of the subcommittee on amphibole of the International Mineralogical Association, Commission on New Mineral and Mineral Names. *American Mineralogist* **82**, 1019–37.

LUDDEN, J., GELINAS, L. & TRUDELL, P. 1982. Archaean metavolcanics from the Rouyn–Noranda District, Abitibi greenstone belt, Quebec, 2. Mobility of trace elements and petrogenetic constraints. *Canadian Journal of Earth Science* **19**, 2276–87.

LUDWIG, K. R. 1993. A computer program for processing Pb–U–Th isotope data, version 1.24, Denver. *United States Geological Survey, Open File Report* 88-542, 32 pp.

LUDWIG, K. R. 2000. *Isoplot/Ex: A geochronological toolkit for Microsoft Excel.* Berkeley Geochronology Center, Berkeley.

LUHR, J. F. 1992. Slab derived fluids and partial melting in subduction zones: insight from two contrasting Mexican volcanoes (Colima and Ceboruco). *Journal of Volcanology Geothermal Research* **54**, 1–18.

MEZGER, K. & KROGSTAD, E. J. 1997. Interpretation of discordant U–Pb zircon ages: an evaluation. *Journal of Metamorphic Petrology* **15**, 127–40.

MUNZ, I. A., WAYNE, D. & AUSTRHEIM, H. 1994. Retrograde fluid infiltration in high-grade Modum complex, South Norway: evidence for age, source, and REE mobility. *Contribution to Mineralogy and Petrology* **116**, 32–46.

NTUNGICIMPAYE, A. & KAMPUNZU A. B. 1987. Caractérisation géochimique des métabasites Kibariennes (Protérozoïque moyen) du Burundi. In *Current Research in African Earth Sciences* (eds Matheis and Schandelmeier), pp. 37–40. Rotterdam: Balkema.

ORMEROD, D. S., HAWKESWORTH, C. J., ROGER, N. W., LEEMAN, W. P. & MENIES, M. 1988. Tectonic and magmatic transitions in the western Great basin, USA. *Nature* **333**, 349–53.

PATIÑO-DOUCE, A. E. 1995. Experimental generation of hybrid silicic melts by reaction of high-Al basalts with metamorphic rocks. *Journal of Geophysical Research* **100**, 15623–39.

PEARCE, J. A. 1982. Trace elements characteristic of lavas from destructive plate boundaries. In *Andesite* (ed. R. S. Thorpe), pp. 525–48. Chichester: Wiley.

PEARCE, J. A. 1983. Role of sub-continental lithosphere in magma genesis at active continental margins. In *Continental Basalts and Mantle Xenoliths* (eds C. J. Hawkesworth and M. J. Norry), pp. 230–49. Nantwich: Shiva.

PEARCE, J. A. & PEATE, D. W. 1995. Tectonic implications of the composition of volcanic arc magmas. *The Annual Review of Earth and Planetary Science* **23**, 251–85.

https://doi.org/10.1017/S0016756804009951 Published online by Cambridge University Press

PHARAOH, T. C. & PEARCE, J. A. 1984. Geochemical evidence for the geotectonic setting of Early Proterozoic metavolcanic sequences in Lapland. *Precambrian Research* **25**, 283–308.

PLANK, T. & LANGMUIR, C. H. 1993. Tracing trace elements from sediment input to volcanic output at subduction zones. *Nature* **362**, 739–43.

PLANK, T. & LANGMUIR, C. H. 1998. The geochemical composition of subducting sediments and its consequence for the crust and mantle. *Chemical Geology* **145**, 325–94.

POLAT, A., KERRICH, R. & WYMAN, D. A. 1998. The late Archaean Schreiber-Hemlo and White River-Dayohessarah greenstone belts, Superior Province: collages of oceanic plateaus, oceanic arc, and subduction-accretion complexes. *Tectonophysics* **289**, 295–326.

PUCHTEL, I. S., HOFMANN, A. W., MEZGER, K., JOCHUM, K. P., SHCHIPASKY, A. A. & SAMSONOW, S. V. 1998. Oceanic plateau model for continental crustal growth in the Archaean: a case of study from Kostomuksha greenstone belt, NW Baltica Shield. *Earth and Planetary Science Letters* **155**, 57–74.

ROLLINSON, H. 1993. *Using geochemical data: evaluation, presentation, interpretation*. Harlow, UK: Longman, 352 pp.

ROMER, R. L. & LEHMANN, B. 1995. U–Pb columbite age of Neoproterozoic Ta–Nb mineralization in Burundi. *Economic Geology* **90**, 2303–9.

RUMVEGERI, B. T. 1991. Tectonic significance of Kibaran structures in central and eastern Africa. *Journal of African Earth Sciences* **13**, 267–76.

SATO, H. 1977. Nickel content of basaltic magmas: identification of primary magmas and a measure of the degree of olivine fractionation. *Lithos* **10**, 113–20.

SAUNDERS, A. D., STOREY, M., KENT, R. W. & NORRY, M. J. 1992. Consequences of plume-lithosphere interactions. In *Magmatism and the Causes of Continental Break-up* (eds B. C. Storey, T. Alabaster and R. J. Pankhurst), pp. 41–60. Geological Society of London, Special Publication no. 68.

SHERVAIS, J. W. 1982. Ti–V plots and the petrogenesis of modern and ophioloitic lavas. *Earth and Planetary Science Letters* **46**, 344–60.

SPEAR, F. S. 1993. *Metamorphic phase equilibria and pressure–temperature–time paths*. Mineralogical Society of America Monograph, pp. 1–799.

STACEY, J. S. & KRAMERS, J. D. 1975. Approximation of terrestrial lead isotope evolution by a two stage model. *Earth and Planetary Science Letters* **26**, 207–21.

SUN, S.-S. & MCDONOUGH, W. F. 1989. Chemical and isotopic systematics of oceanic basalts: implications for mantle composition and processes. In *Magmatism in the Ocean Basins* (eds A. D. Saunders and M. J. Norry), pp. 313–45. Geological Society of London, Special Publication no. 42.

TACK, L., FERNANDEZ-ALONSO, M., TAHON, A. & WINGATE, M. 2002. Meso- and Neoproterozoic emplacement ages of magmatic rocks in Burundi: new constraints for the geodynamic evolution of the "Northeastern Kibaran belt" (NKB). *Abstract Volume IGCP 418/440 (the Kibaran of southwest Africa) technical meeting*, Windhoek, 2002.

WINCHESTER, J. A. & FLOYD, P. A. 1977. Geochemical discrimination of different magma series and their differentiation products using immobile elements. *Chemical Geology* **20**, 325–43.

YARDLEY, B. W. D. 1989. *An introduction to metamorphic petrology*. Longman Earth Science Series, 248 pp.

https://doi.org/10.1017/S0016756804009951 Published online by Cambridge University Press